

UNIVERSITÀ DEGLI STUDI DI NAPOLI “FEDERICO II”



FACOLTÀ DI INGEGNERIA

PhD in Aerospace, Naval and Quality Engineering

XXIII Cycle

**Research on non-conventional working
fluids for space and terrestrial heat pipes**

Ing. Roberto Di Paola

Tutor

Ch.mo Prof. Ing. Raffaele Savino

Coordinatore:

Ch.mo Prof. Ing. Antonio Moccia

Contents

Abstract.....	4
Preface.....	5
<u>1 Heat Pipe and Self-rewetting Fluids.....</u>	<u>7</u>
<u>1.1 Heat pipe</u>	<u>7</u>
<u>1.1.1 Introduction.....</u>	<u>7</u>
<u>1.1.2 Analytical model, Operative limitations and range operation.....</u>	<u>11</u>
<u>1.1.3 Thermal Management</u>	<u>14</u>
<u>1.2 Surface phenomena in liquid-vapour system.....</u>	<u>15</u>
<u>1.2.1 Surface tension.....</u>	<u>15</u>
<u>1.2.2 Surface tension gradient: Marangoni effect.....</u>	<u>18</u>
<u>1.3 Self-rewetting fluids</u>	<u>21</u>
<u>2 Nanofluids.....</u>	<u>23</u>
<u>2.1 Introduction.....</u>	<u>23</u>
<u>2.2 Synthesis and characterization of nanofluids.....</u>	<u>25</u>
<u>3 Measurements of thermo-physical properties.....</u>	<u>29</u>
<u>3.1 Introduction.....</u>	<u>29</u>
<u>3.2 Surface tension measurements.....</u>	<u>29</u>
<u>3.2.1 Experimental Setup</u>	<u>29</u>
<u>3.2.2 Technique of measurement: Algorithm for surface tension measurements.....</u>	<u>39</u>
<u>3.2.3 Measurements results.....</u>	<u>46</u>
<u>3.3 Contact Angle measurements.....</u>	<u>50</u>
<u>3.3.1 Technique of measurement.....</u>	<u>50</u>
<u>3.3.2 Measurements results.....</u>	<u>55</u>
<u>3.4 Thermal conductivity measurements.....</u>	<u>56</u>
<u>3.4.1 Experimental Setup and Measurement Technique.....</u>	<u>56</u>
<u>3.4.2 Measurements Results.....</u>	<u>57</u>
<u>4 Filling procedure and thermal tests of commercial heat pipes.....</u>	<u>60</u>
<u>4.1 Introduction.....</u>	<u>60</u>
<u>4.2 Breadboard for Experimental Setup.....</u>	<u>61</u>
<u>4.3 Filling procedure.....</u>	<u>65</u>
<u>4.4 Results.....</u>	<u>68</u>
<u>4.4.1 Objectives.....</u>	<u>68</u>
<u>4.4.2 Pure Water, Self-rewetting and Self-rewetting nanofluids as working fluid in a commercial groove heat pipe.....</u>	<u>69</u>
<u>4.4.3 Effect of filling ratio on thermal test.....</u>	<u>70</u>
<u>4.4.4 Effect of forced convection on thermal performances.....</u>	<u>73</u>
<u>4.4.5 Comparison between pure water and self-rewetting fluid as working fluid for thermal management of a dummy CPU.....</u>	<u>75</u>
<u>5 Capillary rising in a laser-engraved capillary structure.....</u>	<u>77</u>
<u>5.1 Introduction.....</u>	<u>77</u>
<u>5.2 Laser engraving technique.....</u>	<u>77</u>
<u>5.3 Experimental study on capillary rising in two different groove structures.....</u>	<u>80</u>
<u>5.4 Numerical results</u>	<u>83</u>
<u>6 SELENE Project.....</u>	<u>85</u>
<u>6.1 General description.....</u>	<u>85</u>

6.1.1 Scientific background and motivation.....	85
6.1.2 Justification for the need of a space experiment.....	86
6.1.3 Detailed objectives.....	87
6.1.4 Experiment concept diagram.....	89
6.1.5 Shape, structure and size of heat pipe cell.....	90
6.2 Numerical Simulations.....	92
7 Conclusions.....	96
References.....	97

Abstract

In recent literature one of the most discussed arguments is about the study of such kind of solutions with particular surface properties, the main objective of this work has been focalized on the selection and analysis of innovative working fluids through the measurements of surface tension, contact angle and thermal conductivity properties of different liquids in particular of binary and ternary mixture called “self-rewetting” with an anomalous dependency of surface tension with temperature and concentration. For the first time has been produced another kind of carbon nanoparticles “Nanohorns” and different fluids has been produced with the dispersion of carbon nanoparticles with interesting properties. It has been demonstrated as the use of this kind of solutions (self-rewetting and nanoself-rewetting solutions) improve the thermal performances of two-phase heat transfer device in particular of groove commercial copper heat pipes. Finally a capillary structure has been manufactured with laser-engraving technique in order to evaluate the effect of concentration gradient for a self-rewetting solution in capillary rising.

Keywords: self-rewetting, heat pipe, nanohorn

Preface

This work has been developed during the last three years and it is now presented in the form of final dissertation in partial fulfillment of the requirements for the Ph.D. in Aerospace, Naval and Quality Engineering. The study focused on the self-rewetting fluids, i.e. fluids with unique surface tension properties, as innovative working fluids for heat transfer applications. Self-rewetting working fluids are water alcohols solution that exhibit a reverse Marangoni flow along a liquid-vapor interface. When used as working fluid in two phase heat transfer device, such heat pipes, Marangoni effect driving the liquid towards the hot side increasing the heat transfer limit of the system.

In the first chapter an overview on self-rewetting fluids as innovative working fluid for heat transfer applications is presented.

In the second chapter the synthesis process and characterization of different nanofluids: in particular silver-capped nanofluids produced by Utzonomya university and a new class of carbon nanoparticle has been produced with ENEA research center of Roma (Italy).

In the third chapter surface tension, contact angle and thermal conductivity measurements have been done for all solutions presented: self-rewetting and nanoself-rewetting solutions.

In fourth chapter activities the thermal performances of heat pipes filled with both ordinary and self-rewetting working fluids has been carried out in particular has been evaluated the effect of self-rewetting fluids as working fluid in heat pipe device for thermal management of a dummy CPU.

The fifth chapter has been described the laser-engraving technique for manufacturing of an aluminium grooved structure and the effect of concentration gradient on self-rewetting solution has been studied both experimentally and numerically.

In the last chapter the SLENE project has been introduced and some numerical simulation for the prevision of critical heat flux have been done as first part of one work package of project.

I would like to express my deep appreciation to my tutor Prof. Raffaele Savino for his full support and guidance throughout the course of these three years. I due my thanks to Doctor Yoshiyuki Abe and professor Masahide Sato for their ever clear discussions.

To Dr. Mario De Stefano Fumo and Dr. Diego Paterna, my sincere thanks for their supports and in particular for their friendship.

To Dr. Anselmo Cecere and Mr. Lino Loquace, for their help during the last three years.

My best thanks go to all students that have accompanied me in this period and have taught me so much, just in chronological order: Valerio Carandente, Francesco Capuano, Mario Valente, Francesco Avallone, Antonio Acone, Roberto Russo and my last three students Luigi Iannuzzella, Vincenzo De Santis and Anna Del Prete.

The last and sincere thanks to my family and all my friends !!!

Roberto Di Paola

1 Heat Pipe and Self-rewetting Fluids

1.1 Heat pipe

1.1.1 Introduction

The birth of the heat pipe dates to about 1944 by Graugler. Very little attention was paid to the idea until 1964 when Grover, Cotter and Erickson of Los Alamos National Laboratory described heat transfer experiments with three structures of unique internal construction, which they referred to as “heat pipe”. Since that time, heat pipes have been employed in numerous applications ranging.

A heat pipe is a closed heat transfer system used to transport heat from one location to another by means of the evaporation and subsequent condensation of an appropriate working fluid. It contains three components, the container, wicking structure constructed, and working fluid. The capillary forces in the wicking structure maintain the liquid circulation inside the heat pipe.

A heat pipe is shown in Figure 1-1. The addition of heat along a portion of the container surface (the evaporator section) causes liquid to evaporate. The high temperature associated high pressure result in the flow of the vapour to the cooler condenser region. The removal of heat from some other portion of the surface (the condenser section) causes vapour to condense, giving off the latent heat of vaporization. Depletion of liquid from the wicking structure in the evaporator region causes a difference in capillary pressure (from condenser to evaporator) of the liquid in the wick, as illustrated in Figure 1-2. The differences in the capillary pressure forces the liquid from the condenser back to the evaporator. The wicking structure provides the mechanism by which the working fluid is returned from the condenser to the evaporator, and ensures that the working fluid is evenly distributed over the evaporator surface. To operate properly, the working fluid must wet the wick material and container; that is, the contact angle must be less than 90° .

Heat pipes are highly efficient heat transfer systems in electronics cooling, air conditioning, thermal management of spacecrafts and satellites, propulsion, power generation, energy recovering, chemical engineering and other applications.

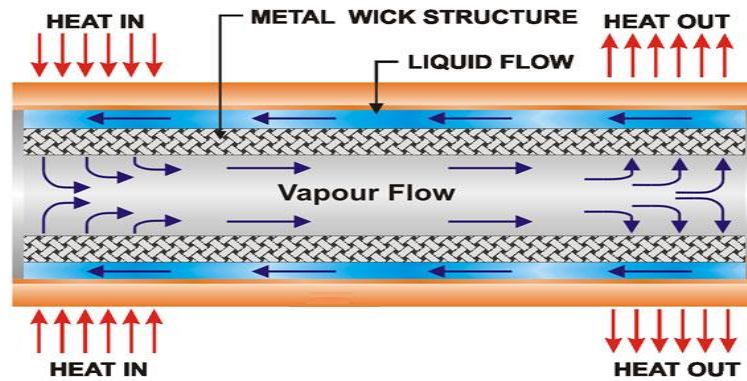


Figure 1-1 Operation scheme of a groove heat pipe

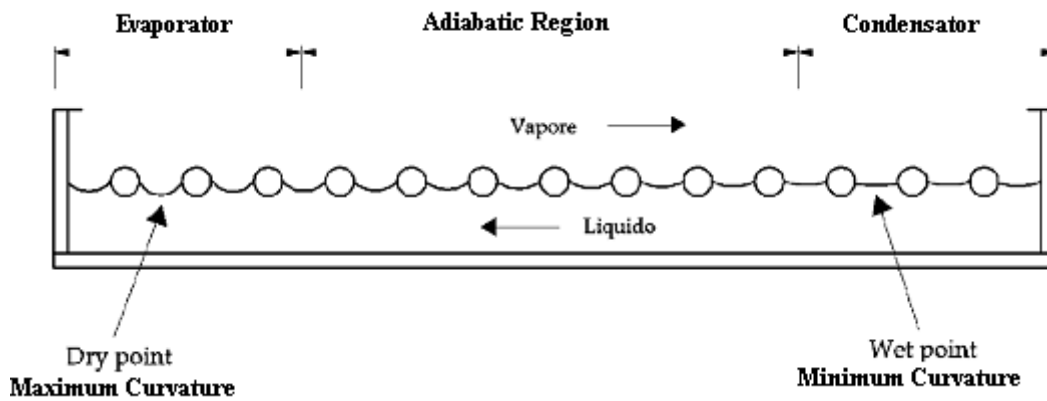


Figure 1-2 Illustration of differences in capillary pressure

Since the latent heat of evaporation is usually very large (about 2.26 MJ/Kg for water), a large amount of heat (several orders of magnitude larger than in conventional convective systems with an equivalent temperature difference) can be transported with a very small temperature difference and with small lightweight structures.

According to the operating temperature ranges of heat pipes are referred to as “Cryogenic” (0 to 150 °K), “Low Temperature” (150 to 750 °K) and “High Temperature” (750 to 3000 °K)[1].

Working fluids are usually elemental or simple organic gases in the cryogenic range, mainly polar molecules or halocarbons in the low temperature range, and liquid metals in the high temperature range. The main requirements for a suitable working fluid are compatibility with the materials forming wick and envelope wall, good thermal

stability, wettability of wick and wall materials, an operating vapour pressure that is not too high or low over the operating temperature range, high latent heat, high thermal conductivity, low liquid and vapour viscosities, high surface tension and acceptable freezing point.

Because of their low-height, zero-maintenance, reliability and high efficiency, heat pipes are highly effective heat transport devices used in spacecraft and other industry branches.

Constant conductance longitudinal-grooved heat pipes, flat heat pipes, variable conductance heat pipes, flexible heat pipes, miniature heat pipes with different materials, different working temperatures, and different shapes and dimensions are developed and manufactured in USA, Japan, Europe, China, etc.

A large number of companies is currently involved in the development and commercialization of this systems. Many companies have been created in the 90s, but some of them have more than 30 years of experience in designing, developing and manufacturing heat pipes, and they have grown since then expanding their market abroad. Their competitiveness lies in developing customized thermal management solutions using the heat pipe technology for many industries including communications, servers/storage, transportation, enclosures, industrial controls, automotive and medical equipment. Some of these companies are listed in Table 1-1.

These companies, however, represent only a fraction of the heat pipes intellectual property market. Smaller companies and individual inventors hold most of the granted and pending patents in the field of heat pipes technology.

Heat pipes Manufacturers	Location
Acrolab Ltd.	USA
ACK Technology, Inc.	USA
Advanced Cooling Technologies, Inc.	USA
Aerocool Advanced Technologies Corp.	China
DAU Ges.m.b.H & CO. KG.	Austria
DAU Thermal Solutions, Inc.	USA
Dynatherm Corporation	USA
Dynatron Corp.	USA
E-Core, Inc.	USA
Enertron, Inc.	USA

Fujikura America, Inc.	USA
Fujikura Europe Ltd, Electronics Division	United Kingdom
Furukawa America Inc.	USA
FURUKAWA ELECTRIC	Japan
Heat Pipe Technology, Inc.	USA
Indek Corporation	USA
InnergyTech Inc.	USA
Isoterix Ltd	United Kingdom
Noren Products, Inc.	USA
Quen Cheer Industrial Co., Ltd.	China
S&P Coil Products	United Kingdom
Swales Aerospace, Inc	USA
Thermacore, Inc.	USA
Thermomax, Inc	United Kingdom
ThermoTek, Inc.	USA
Transterm	Romania
ZETA Electronics Co., LTD	China

Table 1-1: Mayor companies involved on manufacturing and commercialization of heat pipes.

In the geographical distribution of heat pipes manufacturers, the major role is played by USA, as shown in Table 1-1 and Figure 1-3. Other important contributions are given by Europe and China players, which share about 12% of the global market.

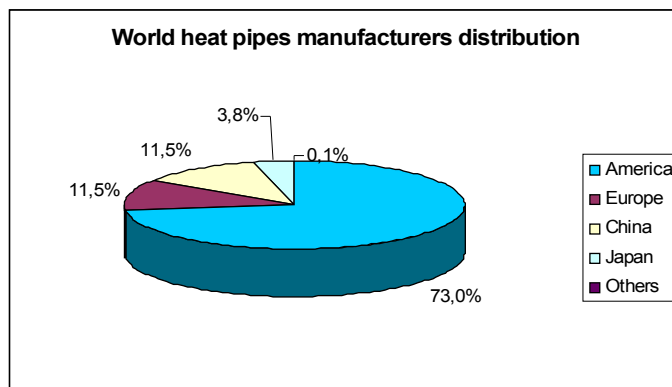


Figure 1-3: Pie chart representing the distribution of intellectual property by geographical

1.1.2 Analytical model, Operative limitations and range operation

As previous shown in Figure 1-2, it is the curvature in the liquid-vapor interface that gives rise to reverse flow of liquid from condenser to evaporator. Interfacial radius of curvature varies continuously along the axis of pipe. The Laplace-Young equation governs the pressure difference between liquid and vapour phases at any point along the axis.

$$P_v(x) - P_l(x) = \frac{\sigma}{r(x)}$$

or, by differentiating wrt x,

$$\frac{dP_v}{dx} - \frac{dP_l}{dx} = -\frac{\sigma}{r^2} \frac{dr}{dx}$$

Along the X axis, the x=0 being fixed at the evaporator end, if vapour temperature is assumed constant and if vapour is treated like an ideal incompressible gas, then from Clapeyron equation [2].

$$\Delta T \approx T_{sat}^2 \Delta P / P_{sat}$$

This equation gives a very small change in the vapour pressure along the axis. Now, in the differentiated Laplace-Young equation, vapor pressure gradient is a very small negative number (zero, under our strict assumptions) and gradient in r(x) is positive because there should not be any sign changes in the pressure gradient along the axis. As a result, we have a positive liquid pressure gradient, which is actually responsible for driving the flow from the condenser to evaporator along the channel in wick structure.

The physical process occurring during the transport of the heat input impose a number of constrains on heat pipe operation. The limitations are:

A. Capillary limit.

It describes the ability to circulate or pump the given working fluid inside the heat pipe. Sometimes it is called Hydrodynamic Limitation. It also defined as the maximum circulation inside the micro heat pipe in order to obtain the maximum heat capability. The capillary limitations of heat pipe occurs when the capillary pressure difference in the liquid phase is not great enough to overcome the sum of the pressure drops associated with

the liquid flow, vapour flow, and phase change phenomena. This can be resumed with a simple equation:

$$\Delta P_c \geq \Delta P_+ + \Delta P_{\parallel} + \Delta P_l + \Delta P_v$$

Where

ΔP_c = net capillary pressure difference

ΔP_+ = radial hydrostatic pressure drop

ΔP_{\parallel} = axial hydrostatic pressure drop

ΔP_l = viscous pressure drop in liquid phase

ΔP_v = viscous pressure drop in vapor phase

B. Sonic limit

It occurs when the sonic velocities are reached in the vapour flow, leading to a choked flow condition in some parts of the heat pipe, usually at the start of the condensation zone.

C. Viscous limit

This limit appears in regard to the fraction in the vapour flow at low temperature limiting the circulation of the working fluid. It occurs when vapour pressure is not sufficient to drive the vapour phase from the evaporator region to the condenser region of the heat pipe.

D. Boiling limit

It is the disruption of the liquid flow by nucleate boiling in the sharp corners when intense heat flux level in the evaporator region lead to the formation of vapour bubbles.

E. Entrainment limit

It is tearing of liquid off the liquid-vapor interface by vapour flow at high velocity. It is reached when the vapour shear stress tend to remove liquid from the liquid flow channel, leading to premature dry-out of the evaporator region.

F. Vapor continuum limit

When the vapour loses property as continuum fluid. [3] defined the vapour continuum limit in terms of Knudsen number. If Knudsen ration is less or equal to 0.01, the vapour sustains its characteristics as continuum fluid in the heat pipe.

Relatively to the operation of heat pipe, a great relevance is not only the working fluid but also the wick structure, in fact it can be homogeneous (axial groove, arterial groove, etc.) or composite (screen mesh, wire, etc.). Each has advantages and drawbacks, see Table II.1.2.

Wicking material	Conductivity (straight)	Overcome gravity	Thermal resistance	Stability	Conductivity lost
Axial groove	Good	Poor	Low	Good	Average
Screen mesh	Average	Average	Average	Average	Low
Fine fiber	Poor	Good	High	Poor	Average
Sintetering (powered)	Average	Excellent	High	Average	High

Table II.1.2 Propriety of wick materials

The temperature range, generally between the triple point and the critical point of the working fluid, determine the choice of the working liquid. The container must be lightweight, compatible with the working fluid and must exhibit good thermal conductivity.

The simplest heat pipe is a cylindrical straight pipe which is easy to fabricate and has a low cost of production. Other type of heat pipe are also manufactured. For the flat heat pipe the increased in surface area to volume ratio maximize power density, meaning the thermal power carried from evaporator to condenser . Additionally their flat surfaces allow for better thermal contact as well as the ability to stack or layer the heat pipe with other systems (e.g. photovoltaic cells) on both sides. They are typically used for cooling printed circuit boards or for heat levelling to produce an isothermal plane. In some applications several flat heat pipes are sandwiched together. In general the thermal resistance increases as the heat pipe becomes more flat, thereby tending to reduce thermal performances.

Flexible heat pipes allow for misalignment between heat source and heat sink and can be successfully employed in presence of oscillations and vibrations. Furthermore, flexible systems can be very useful in some applications where relative motion is required (e.g. between movable portions of computers, such as base section and a LCD display of a laptop [4]).

The first “0-g” demonstration of a heat pipe was conducted on the 1967 by a group of engineering of the Los Alamos Scientific Laboratory. Actually, heat pipe are extensively used from the aerospace designers to solve the ever-present temperature control problems on spacecraft. Their principal function is to transport heat from dissipative equipment to radiative panels.

1.1.3 Thermal Management

Most of heat pipe for space application have axial grooves wick structure and are made of extrude aluminium 6063. The common working fluid is ammonia as its operational temperature is well suited to space applications (-40, 80 °C) [5]. Axially grooved heat pipes offer relatively simple industrial fabrication and greater reliability than other wick designs, such as artery heat pipes.

Space environment demands that heat pipes respond to particular features:

- high thermal conductivity,
- lightweight and compact design,
- uniform temperature
- autonomous and reliable concept with no maintenance.

Typical heat pipe performance for space application’s are listed in Tab. II.1.3.

Diameters (<i>mm</i>)	(8 – 25)
Lengths (<i>m</i>)	0.25 – 4
Linear mass (<i>g/m</i>)	350/670
Heat Transport capacity (<i>W m</i>)	50/600
Maximum heat flux density (<i>W/cm²</i>)	3/10
Operating temperature range	-40, 80
Life time (years)	15/20

Tab. II.1.3 Typical heat pipe performance for space applications

Future missions will require extended heat pipe performances, in particular improvement of the heat transport capacity of at least 15% -30 % and the extension of the maximum operating temperature range to 150°C.

This kind of technology based on heat pipes nowadays is also hugely diffused in terrestrial field in several applications; one of the last and future applications is as core of solar panel technology for the problem of air-conditioning of skyscraper and also in order to solve the problem of overheating of modern CED.

1.2 Surface phenomena in liquid-vapour system

1.2.1 Surface tension

In a liquid, surface tension is caused by the attraction between the molecules by various nature intermolecular forces. In the bulk of the liquid each molecule is pulled equally in all directions by neighboring liquid molecules, resulting in a net force of zero. At the surface of the liquid, the molecules are pulled inwards by other molecules deeper inside the liquid but they are not attracted as intensely by the molecules in the neighboring medium (be it vacuum, air or another liquid). Therefore all of the molecules at the surface are subject to an inward force of molecular attraction which can be balanced only by the resistance of the liquid to compression. Thus the liquid squeezes itself together until it has the locally lowest surface area possible.

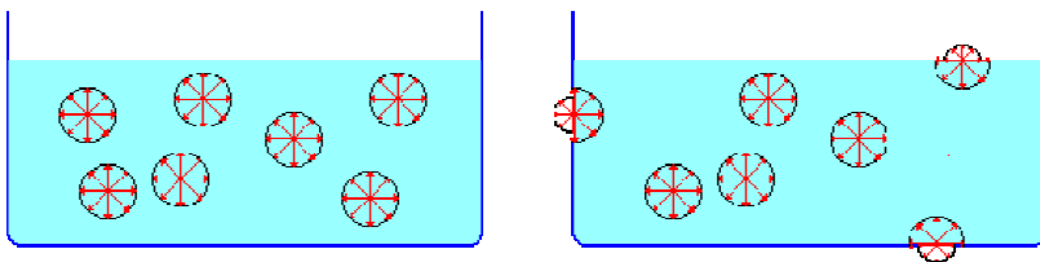


Figure 1-4: Molecular interactions between liquid and ambient phase

Another way to think about that is that a molecule in contact with a neighbor is in a lower state of energy. Interior molecules all have as many neighbors as they can: but the boundary molecules have fewer than interior molecules and are therefore in a higher

state of energy. In order to minimize its energy state, liquid must minimize its number of boundary molecules and therefore its surface area.

As a result, the surface will assume the smoothest and flattest shape it can, because mechanical systems always try to find a state of minimum potential energy. A free droplet of liquid assumes a spherical shape, corresponding to the minimum surface area for a given volume.

Surface tension can also act on external object like an elastic force: since any curvature in the surface shape results in higher area, a strain causes a higher energy state that generates the force. Consequently, the surface will push back on the disturbing object in much the same way a ball pushed uphill will push back to minimize its gravitational energy .

A definition of surface tension, from its thermodynamics point of view, is work done or energy per unit area. As such, in order to increase the surface area of a mass of liquid of an amount, δA , a corresponding energy, " $\sigma \delta A$ ", is needed. Therefore surface tension is usually measured in joules per square meter ($\text{J}\cdot\text{m}^{-2}$), or erg per square centimeter ($\text{erg}\cdot\text{cm}^{-2}$) in the cgs system, but also as a force for unit length, dyne per cm ($\text{dyne}\cdot\text{cm}^{-1}$).

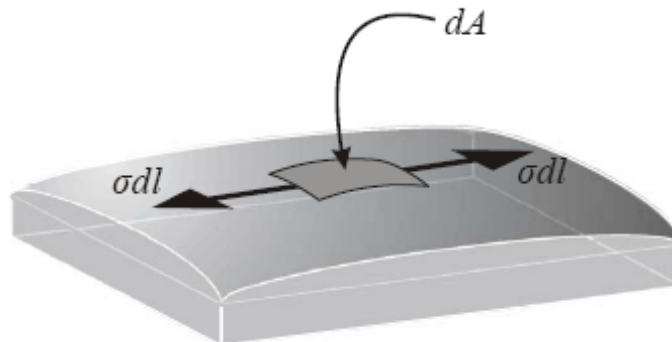


Figure 1-5: Surface tension forces on isotherm interface liquid-vapour

As stated above, the energy necessary to increase a surface is:

$$dW = \sigma dA$$

For a reversible process, $dG=VdP-SdT+\sigma dA$, therefore at constant temperature and pressure, surface tension equals Gibbs free energy per surface area:

$$\sigma = \left(\frac{\partial G}{\partial A} \right)_{p, T},$$

where “G” is Gibbs free energy and “A” is the area.

From the definition it is easy to understand that decreasing the surface area is always spontaneous ($\Delta G < 0$), on the contrary, in order to increase its surface a certain amount of energy is needed, as the process is, per se, non-spontaneous ($\Delta G > 0$). A measure of how spontaneous (or non-spontaneous) is the change in the surface area is precisely the surface tension.

The definition of Gibbs free energy can be arranged to

$$H = G + TS$$

so partial derivation yields

$$\left(\frac{\partial H}{\partial A} \right)_p = \left(\frac{\partial G}{\partial A} \right)_p + T \left(\frac{\partial S}{\partial A} \right)_p$$

and applying the equations of state

$$\left(\frac{\partial G}{\partial T} \right)_{p, T} = -S$$

we obtain

$$\left(\frac{\partial \sigma}{\partial T} \right)_{p, T} = -S^A,$$

where S^A means entropy per surface area [6].

The surface tension value depends on several parameters: in particular we will consider liquid mixtures with a surface tension function of composition and temperature

$$\sigma = \sigma(c, T)$$

where “c” is concentration and “T” is temperature.

1.2.2 Surface tension gradient: Marangoni effect

The simplest method to explain the Marangoni effect is to consider the usual dependence of the surface tension with temperature: in fact for all pure liquids σ is an almost linear decreasing function of temperature (Figure 1-6).

Silicon oil 3 cSt

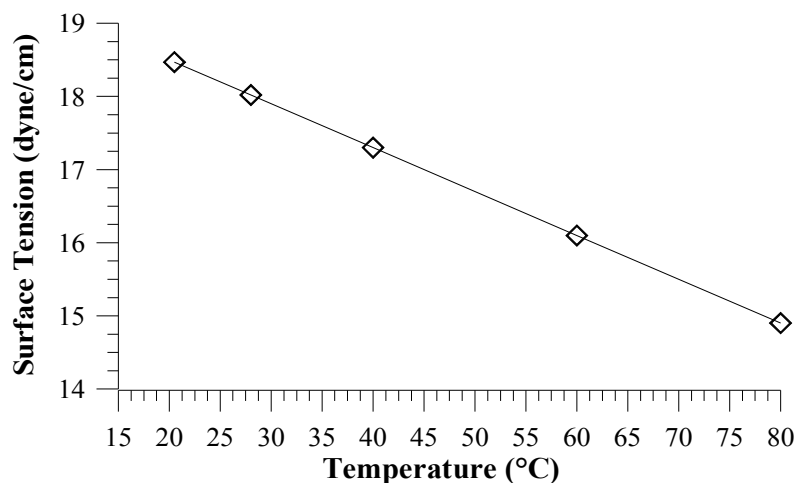


Figure 1-6 Surface tension of silicon oil 3 cSt

When there is a difference of temperature on a liquid surface, we have consequently a surface tension gradient: higher value for cold region, smaller values for hot ones.

We suppose $T_1 > T_2$, so that with reference to the portion of liquid surface shown in Figure 1-7, we have $\sigma(T_1) < \sigma(T_2)$ and correspondingly a surface tension unbalance.

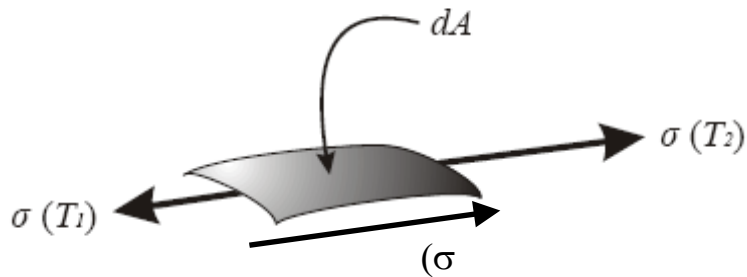


Figure 1-7 Unbalanced surface tension forces for difference temperature at liquid interface

This surface tension gradient ($\nabla\sigma$) is the driving force for “Marangoni convection”: consisting in a convective flow of particles from the hot side towards the cold side for most common liquids, for which the surface tension is a decreasing function of the temperature.

In Figure 1-8 we have represented the velocity distribution in the boundary layer adjacent to the interface: the surface velocity is caused by surface tension gradient and the velocity decrease increasing the distance “y” is the liquid viscosity “ μ ”.

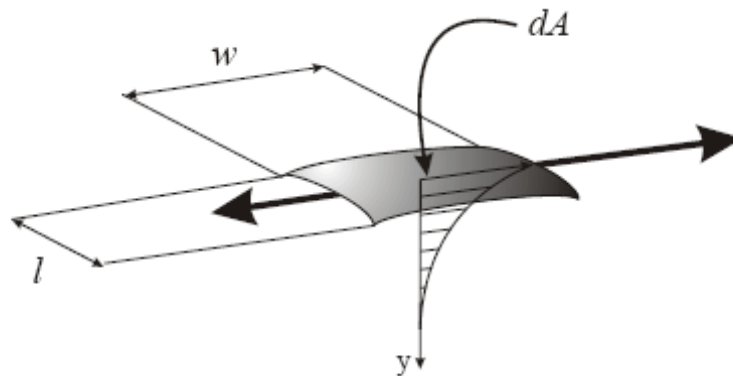


Figure 1-8 Velocity profile generated by Marangoni effect

The momentum balance equation along the interface corresponds to the equilibrium between surface tension force and shear stress:

$$w \Delta \sigma = w l \mu \left(\frac{\partial v}{\partial y} \right)_{y=0}$$

which can be also written in differential form as:

$$\mu \left(\frac{\partial v}{\partial y} \right) = \frac{\partial \sigma}{\partial x}$$

The above equation provides the expression for the Marangoni velocity

$$v_m = \frac{\Delta \sigma}{\mu}$$

If we assume a linear dependence of the surface tension with temperature:

$$\sigma = \sigma_0 + \sigma_T \Delta T$$

$$\Delta \sigma = \sigma_T \Delta T$$

So that the above relation leads to the classical equation for the characteristic thermal Marangoni speed

$$v_m = \frac{\sigma_T \Delta T}{\mu}$$

As pointed out before, for liquid mixtures, the surface tension can strongly depend not only on temperature but also on concentration and, in particular conditions, the surface tension gradient can be directed opposite to the usual case represented in Figure 1-7, i.e. from the cold to the hot side. This subject will be introduced in the next paragraph.

For these reasons, in particular conditions of temperature, pressure and liquid mixture, the surface tension gradient could be in opposite respect previous considerations (Figure 1-7); it will be object of next paragraph.

1.3 Self-rewetting fluids

So called “self-rewetting” fluids are particular liquid mixtures an unusual dependence of the surface tension with temperature other than a dependence of the surface tension one with concentration.

According to Abe in “About of self rewetting fluids- possibility as a new working fluid”, there are three possible situations for liquid mixtures [7] (Table 1-2)

	Single Component	Positive mixture	Negative mixture	Self-Rewetting
$\frac{\partial \sigma}{\partial T}$	<0	<0	<0	>0
$\frac{\partial \sigma}{\partial c}$	---	>0	<0	>0

Table 1-2 Classification of fluids from surface tension behaviour

Binary solutions with usual dependence of the surface tension with temperature,

i.e. with $\frac{\partial \sigma}{\partial T} < 0$, like a single-component liquid, are referred to as “positive” or “negative” mixtures according to whether the surface tension is an increasing or decreasing of the concentration of the less volatile component (i.e. $\frac{\partial \sigma}{\partial c} > 0$ or $\frac{\partial \sigma}{\partial c} < 0$).

For instance, a binary solution of water and ethanol is a positive mixture, because the mixture surface tension is a decreasing function of T and the surface tension increases if the water concentration is larger.

Self-rewetting fluids are mixtures with both surface tension derivatives positive. This particular property makes these fluids very usefull particularly as a working fluids for heat transfer devices.

Fluids already classified as “self-rewetting” are alcohol aqueous solutions with a number of carbon atoms in the alcohol molecule greater then or equal to four: e.g. solution of water and butanol, pentanol, hexanol, heptanol .octanol, etc.

In this case of binary mixtures, two additional forces can be identified at the film vapour interface: thermal marangoni effect (discussed previously) and solutal marangoni effect due to the concentration gradient. Both these effects can oppose or favour the film motion towards the hot end.

The influence of surface tension-driven flows unbalance in heat transfer devices has received attention in the literature [8-14]. Eninger and Marcus [8] proposed the thermal Marangoni effect as the primary mechanism responsible for the observed degradation in axially grooved heat pipes with non-condensable gases. The main speculation was that the temperature –induced surface tension gradient in the condenser region could drive a re-circulatory flow with consequent pressure drop that negatively affects the capillary pressure available to pump the condensate return at the evaporator.

In the case of non-azeotropic composition of self-rewetting mixtures, a decrease in the concentration of more volatile component near the heater surface in well-developed nucleate boiling regime results in an increase in the temperature near the heater surface, as schematically depicted in Figure 1-9. Since the surface tension of most of fluids decreases with the increase in temperature, such a temperature increase may weaken the Marangoni effect induced by the concentration gradient, this do not happened in the case of self-rewetting fluid because of the surface tension derivative with he temperature is positive. In this case we can expect that the Marangoni Flow directed towards hot region is stronger overcoming the problem of instability in liquid flow.

In this work will be presented the effect of using a self rewetting fluids as working fluid in commercial grooved heat pipe and experiments on capillary rising with an home-made capillary structure in order to observe the only effect of solutal marangoni on this kind of mixtures.

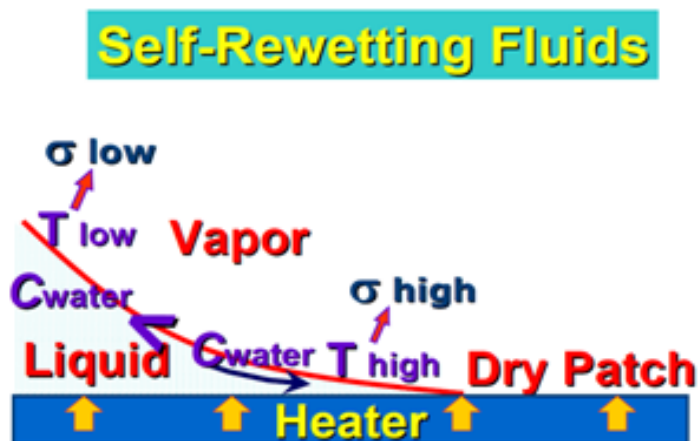


Figure 1-9 Effect of using self-rewetting fluids as worng fluids in two-phase heat transfer devices

2 Nanofluids

2.1 Introduction

Just as downsizing is a fashion in the world of business, downscaling is a clear trend in the world of science and technology. As the age of “bigger is better” gives way to the age of “smaller is better,” microelectromechanical systems (MEMS) technology and nanotechnology are rapidly emerging as the new revolution in miniaturization. One feature of these rapidly emerging technologies is that they are strongly interdisciplinary. In the coming micro- and nanoage, the miniaturization technology with unforeseen applications is expected to revolutionize many industries.

A variety of micro-scale products are already available, or soon will be. Miniaturized sensors, actuators, motors, heat exchangers, pumps, heat pumps, valves, heat pipes, fuel cells, instruments, medical devices, robots, and airplanes are just a few of the almost endless variety of micro products in the market or poised to move from the laboratory to the marketplace. These micro components will also be integrated to build complex MEMS and other systems.

Miniature heat exchangers have numerous attributes, including high thermal effectiveness, high heat transfer surface-to-volume ratio, small size, low weight, low fluid inventory and design flexibility. Because their microchannel systems are extremely compact and lightweight compared to conventional systems, materials and manufacturing costs could be lowered, an attractive advantage that would draw the interest of many manufacturing firms. For example, the electronics industry has applications in cooling advanced electronic packages; for the automotive industry, the weight difference between conventional and microchannel systems (such as in air conditioners) could lead to significant gains in fuel economy: in the HVAC industry).

Refrigeration and air conditioning equipment volumes could be reduced and this would save space in buildings; and in chemical and petroleum plants. plant size could be reduced through “process intensification.” The trend toward miniaturization is also apparent in the U.S. Space

Program, which is developing ultralight spacecraft using MEMS, and in energy industries that are designing microcogeneration systems (1-10 kWe) using micro gas turbines and micro engines.

From virtual obscurity about a decade ago, nanoscience and nanotechnology have entered the limelight [15]. Recent reviews of research programs on nanotechnology in the U. S., China, Europe, and Japan show that nanotechnology will be an emerging and exciting technology of the 21st century and that universities, national laboratories, small businesses, and large multinational companies have established nanotechnology research groups or interdisciplinary centres that focus on nanotechnology [16-19]. It is estimated that nanotechnology is at a similar level of development as computer/information technology was in the 1950s.

Nanomaterials have unique mechanical, optical, electrical, magnetic, and thermal properties.

After nanotechnology will come a technology for building up systems and structures from atoms and molecules via nanoparticles, nanotubes, and nanolayers. One can imagine that once scientists and engineers reach the atomic and molecular scale, they will be able to build systems and structures by using bottom-up methods, starting from atoms and molecules, rather than current top-down methods such as micromachining, lithography, and etching.

Nanofluids that are a new class of solid-liquid composite materials consisting of solid particles, with size typically in the order of 1-100nm, suspended in a heat transfer fluid. The potential of this class of fluid is related to their higher thermal conductivities compared to their base fluids for over the past decade [20,21]. Common base fluids include water, ethylene glycol, transformer oil and toluene. Nanoparticles are typically made of chemically stable metals, metal oxides or carbon in various forms. The significant enhancement of thermal conductivity for a variety of nanoparticle/fluid system has been reported by many researchers. Also, several researches in convective heat transfer [22-24], boiling heat transfer [25,26] using nanofluids were investigated. More recently, some researchers reported the thermal performance of heat pipes with gold [27] and silver [28,29] nanoparticles dispersed nanofluids, and their results show that the thermal resistance of heat pipe with both types of nanofluids is lower than that of pipes containing pure water.

Other authors suggested the preparation of nanofluids by using carbon nanostructures. Multi-wall carbon nanotubes carbon nanofibers have been used. In this work SWNH and Silver capperd have been used to produce self rewetting nanofluids.

The main idea is to combine both class of heat transfer fluids: self rewetting fluids and nanofluids.

2.2 Synthesis and characterization of nanofluids

There are several technique reported in the literature for the synthesis of novel forms of carbon based nanostructures: laser ablation, chemical vapour deposizion and arc discharge. The last one has been utilized in order to produce a new form of carbon nanoparticle, named Single Wall Nanohorns.

These structures appear particularly suitable for preparing nanofluids due to their very low dimensions (aggregates with diameters in the range 20-100 nm) and to their chemical surface properties which are at the base of an improved dispersion capacity in many liquids. The use of arc discharge has demonstrated that it is possible to produce this carbon nanostructure in a simple and cheap way. SWNH have been produced by an alternating current (AC) fed arc discharge with a symmetric configuration of the electrodes. By this way it has been maximized the quantity of evaporated material which can be collected as fine soot. In fact in the case of direct current (DC) fed arc discharge the formation of the hard crust on the cathode, which contains Multi-Wall carbon Nanotubes and polyhedral graphitic structures, could not be avoided [30]. In this case about 75% of the total weight of sublimated graphite is collected in the crust. When the arc is fed by an AC arc discharge quite only the soot containing SWNH is produced and the remaining sublimated graphite is lost by the formation of gaseous byproducts [31]. For this work two pure graphite electrodes 6 mm in diameter have been arched in vertical geometry when 28 V were applied at their extremities. The frequency of the feeding current was 35 Hz. As reported in a previous work the frequency affects the structural characteristics of the material produced in particular at 35 Hz the production of dahlia-like SWNHs was higher respect to higher values of the frequency [32].

The electrodes sublime during the arc due to very high temperatures reached and for this reason one of the electrodes is moved at a fixed velocity toward the other. In this way the arc is stable and continuous for a long time. Moreover the consumption of the electrodes is quite the same.

Near the arc zone it has been fixed a cylindrical stainless steel collector as represented in Figure 2-10.

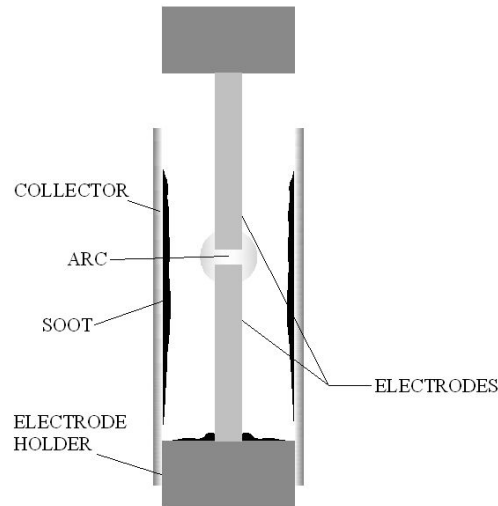


Figure 2-10: Simple scheme of the apparatus used for the arc discharge

The collector is useful to collect the material produced during the arc discharge. The soot adheres on its inner wall and it could be easily recovered after the experiment. During the experiments conducted in the past it has been demonstrated that the role of the collector is multiple: on one side it recovers the material with quite homogeneous characteristics, on the other side it has an important role in governing the thermal characteristics of the zone near the arc, in particular it reduces drastically thermal losses due to convection.

The arc is performed in air and no vacuum or gas line is needed.

The electrodes sublimated are made of pure graphite and pure carbon based structures can be produced by this method. This feature is particularly important because principally the type of structure influences the measurements of thermal conductivity performed on nanofluids dispersing this material in different solvents.

The as prepared material has been observed by scanning and transmission electron microscopy. In Figure 2-11 SWNH aggregates can be observed which form chains like in carbon black. Also in this case a primary particle constituted by SWNH aggregated can be observed.

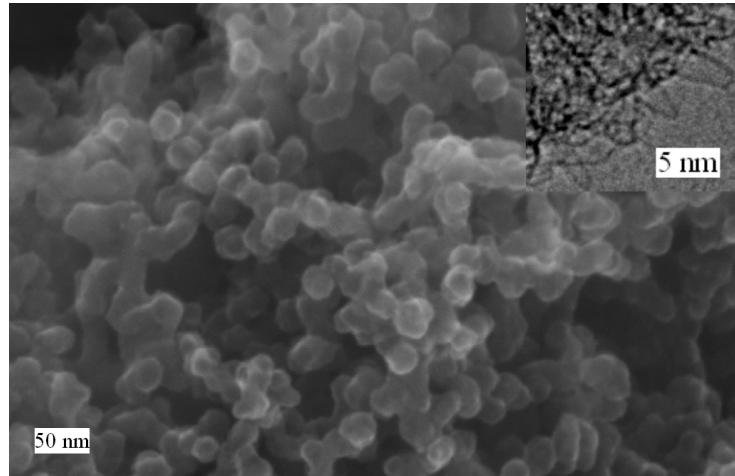


Figure 2-11: Aggregates of SWNH produced by arc discharge observed by field emission scanning electron microscope

In order to prepare nanofluids the soot has been dispersed in water with 5wt% of butanol in an ultrasonic bath for 20 minutes. Surprisingly the suspension has revealed to be very stable during a long time: no deposit or floating material could be observed after many days. This time is orders of magnitude shorter respect to the time needed to perform thermal conductivity measurements.

Another class of nanofluid that has been studied in this work are silver capped nanofluids produced by University of Utsunomiya in Japan.

In Figure 2-12 shows SEM photographs and outlooks (half-transparent, bright yellow or white-yellow colored) of five different PVP capped silver nanofluids prepared by MW assisted polyol method.

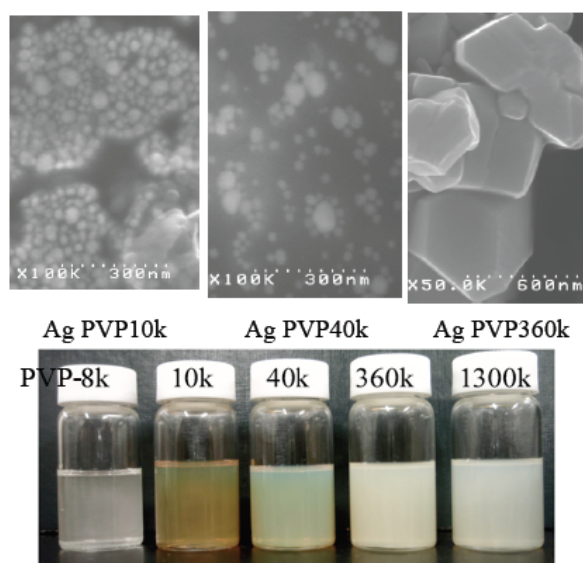


Figure 2-12: SEM photographs and solution colors of AG Nanofluids

The average particle diameter of PVP10k, 40k, 360k and 1300k capped silver nanoparticles is around 40, 100, 300 and 300 nm, respectively, which is corresponding to SEM image shown in Figure 2-12, and these nanofluids keep the long-term (over 6 months) dispersion stability. On the other hand, in the case of PVP8k-capped silver nanofluid, large precipitations were observed within a few hours.

Temperature dependencies of viscosities of 1-butanol-containing silver nanofluid are shown in Figure 2-13.

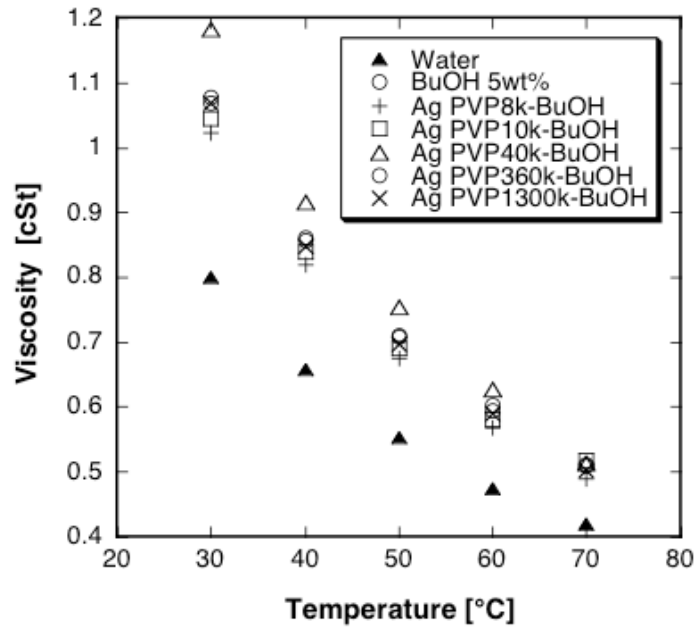


Figure 2-13: Effect of temperature on viscosities of several self-wetting nanofluids.

Prasher et al. reported on viscosities of alumina-based nanofluids and their experimental results suggest that the increase in the nanofluid viscosity is higher than the enhancement in the thermal conductivity to make the nanofluid thermal performance worse than that of base fluid [33]. In contrast, viscosities of Ag nanofluids in the present case were almost same as base fluid 5 wt.% 1-butanol aqueous solution because of dilute silver nanoparticle concentration.

3 Measurements of thermo-physical properties

3.1 Introduction

In consequence of observations have been made about the operating system of heat pipe, the results in term of requirements of working fluid for two-phase heat transfer devices are:

- Good wettability with wick structure and wall
- High Latent Heat of Vaporization
- High thermal conductivity
- High Surface tension

In this chapter will be presented the results of surface tension, contact angle and thermal conductivity measurements performed in the microgravity fluidynamic of Department fo Space Engineer of University of Naples Federico II.

Each paragraph will be organized on an introduction of experimental setup and technique of measurement and in the end the results.

Several liquid mixtures have been measured (binary and ternary) and also the nanofluids that are just considered in previous paragraph.

3.2 Surface tension measurements

3.2.1 Experimental Setup

Experimental setup is composed by

- Experimental cell
- Thermal control system
- Temperature acquisition system
- Tensiometer
- Personal computer for visualization, acquisition and direct control of experiment

The experimental system is based on the Dataphysics OCA 15 tensiometer, characterized by an electronic injection system with a vertical controllable syringe that allows to inject a liquid pendant drop into an optical glass cuvette (with inner dimensions: 9.5mm x 9.5mm x 43.5mm). The cell is partially filled with the same liquid, in order to obtain a saturated vapour at each temperature and to overcome problems related to possible liquid evaporation at relatively high temperatures. The bottom wall of the cell is heated with a Peltier element, in combination with a power supply and a water circulating system, so that the temperature of the surface is constant and controlled (with an accuracy of 0.1°C in the range 20°C - 100°C) during the experiments. A thin thermocouples was used to measure the temperature close to the pendant drop surface. The measurements have been performed in the temperature range of 20 – 80°C.

All subsystems have a particular importance for the surface tension measurements: in fact for liquid mixture with a component more volatile than the other one, many parameters influence the measurement, e.g. stability of liquid mixture (evaporation problems), temperature, perfect condition of field of view of camera, but all this aspects will be reported in the following paragraphs.

The experimental cell is divided in two subsystems:

- An optical glass cell, used as container of liquid (Figure 3-15)
- An external structure (Figure 3-16), realized by our group and formed by several material (it will be better described next), where is allocated the glass cell, so that it's possible to realize and control all measurement parameters.

The glass of optical cell has very good optical properties: above all both refractive and dispersion index are very low, which guarantee a transmission in visible spectrum approximately of 80%. These characteristics are very important for a correct measurement of surface tension as shown in the following paragraphs.

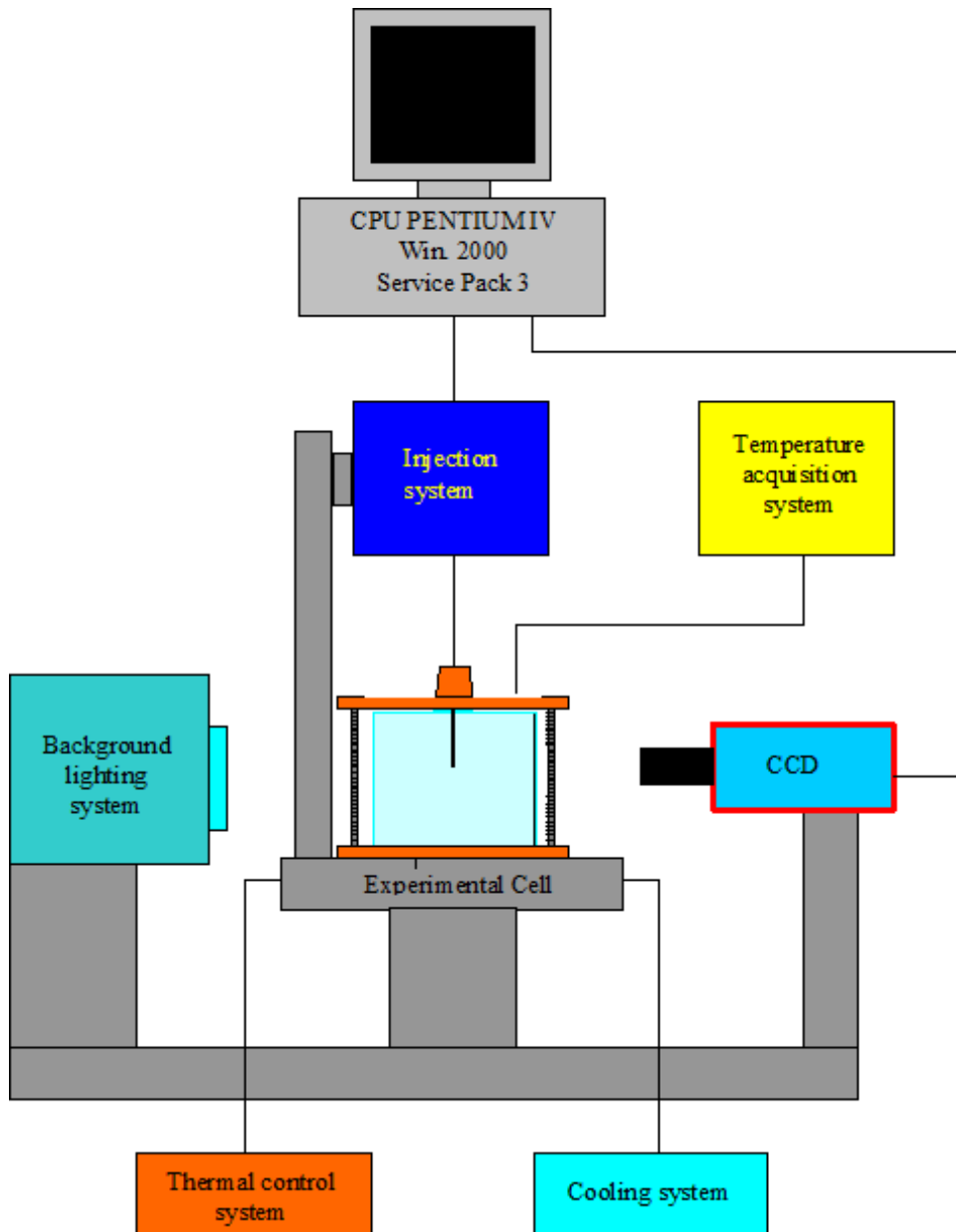


Figure 3-14: Experimental configuration with all subsystems

The external structure is formed by two copper plates, one below and one over the glass cell: the over one is pierced for putting in the needle and the thermocouple. All subsystem is perfectly sealed because the atmosphere in the glass cell has to be controlled without interference or unsteady phenomena.

The plate below is the base of the experimental cell and is joint to the thermo-regulated plate of tensiometer: for a better thermal conductivity between the copper plate and thermo-regulated plate there is a high thermally conductive paste of Omegatherm Society and which properties are showed in the Table 3-3.

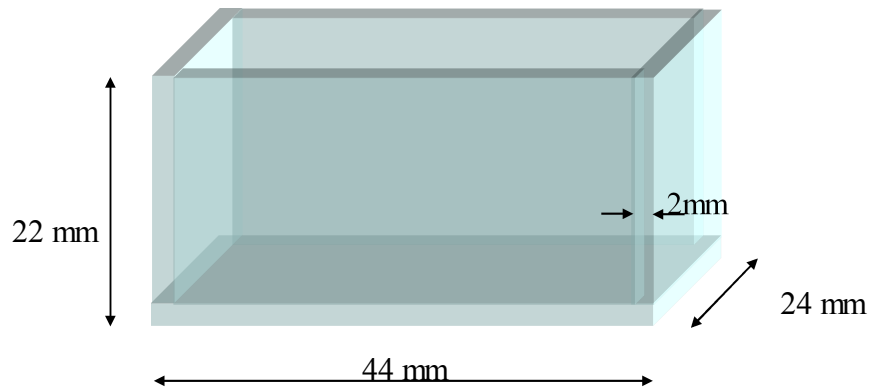


Figure 3-15: Optical glass cell

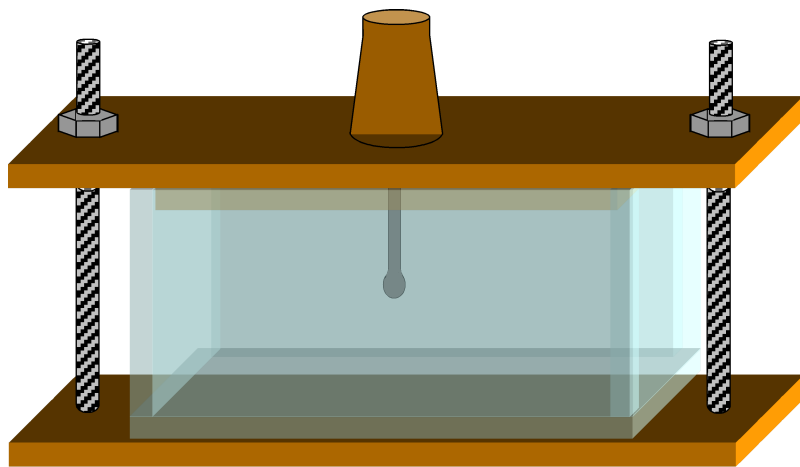


Figure 3-16: External structure where is allocated the glass cell

Model No.	OT-201
Material	Silicone Grease
Continuous Temperature	200°C (392°F)
Cure	Not required
Adheres to Most*	Wets most Surfaces
Thermal conductivity (k)(BTUin)/(hr)(ft 2) (°F)	Extremely High 16
Electrical Insulation Volume Resistivity ohm-cm	Very High 10 ¹⁴

Table 3-3: Technical characteristics of high thermally conductive past Omegatherm



Figure 3-17: Thermal control system TC 400/NHD

The thermal control is realized by a unit control (Figure 3-17). Temperature must be manually set on the screen of TC 400: it is a power supply which controls the peltier element in the thermal-regulated plate of tensiometer. A peltier's side is in contact with the base of the experimental cell while the other one is cooled by circulating water.

The temperature acquisition system is composed by two elements:

- Thermocouples RS 219-4315 (Figure 3-18 (b)), type K using nickel alloys. The operating temperature range, composition and accuracy is defined in IEC 584 (code for temperature measurement, using thermocouples):

Composition -ve arm	Ni 95% balance AL, Si, Mn
Composition +ve arm	Ni 90% Cr 10%
Continuous range temperature	-50°C to +250°C
Accuracy	±1°C

The colour coding for thermocouple wiring and cables is defined in BS4937 part 30 1993 Figure 3-18(a) (British Standard colour code for twin compensating cables for thermocouples).

- A digital thermometer is the 50D model of FLUKE society which use J and K thermocouples and its characteristics are listed in the table below.

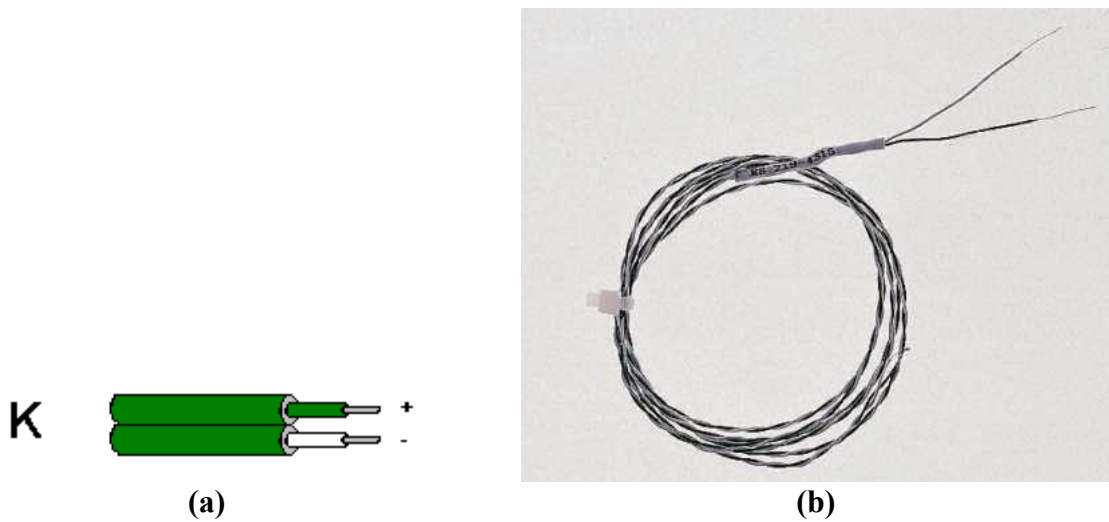


Figure 3-18:

- (a) Colour coded to BS4937 Part 30 1993 for K type thermocouple [34]
- (b) Picture of thermocouple used for temperature acquisition

FLUKE 50D Digital thermometer
Rugged holster protects thermometer
OFFSET function minimizes thermocouple errors
K- or J-type thermocouple compatibility
°C or °F readout
User selectable 0.1 °C (0.2 °F)
HOLD Mode freezes display for convenient viewing
(T1-T2) true differential display mode
SCAN Mode cycles display through T1, T2, (T1-T2)
MIN/MAX Recording

Table 3-4: Digital thermometer characteristics
[\[http://www.tequipment.net/FlukeThermo50D.html\]](http://www.tequipment.net/FlukeThermo50D.html)

The tensiometer is studied for surface tension and contact angle measurement; it's possible to use several techniques for this scope, in particular for surface tension measurement. The tensiometer "OCA 15+" of Dataphysics society (Figure 3-19) can use four methods:

- Lamella method
- Pendant Drop method

The lamella method is based on the balance of power between the surface tension and the force of gravity. A liquid lamella will shape if we bring a vertical test piece in contact with a liquid. Based on Young-Laplace differential equation the surface tension can be calculated if the contour of the lamella and the force of gravity are known.

The method chosen in this work is the last one. A liquid drop is injected in the cell with a syringe controlled by software. In this condition the shape of the drop is defined by the equilibrium of two forces:

- 1) The gravitational force which lengthens the drop in the same direction of gravity field
- 2) The surface tension which imposes a spherical shape of the drop

The equilibrium of these forces is defined by the Young-Laplace equation in which the pressure difference across the liquid-vapour interface is related to the radius of curvature, to the side of the drop, to the density and to the surface tension. From the density and the drop shape it is possible to evaluate the surface tension of test liquid at a given temperature.

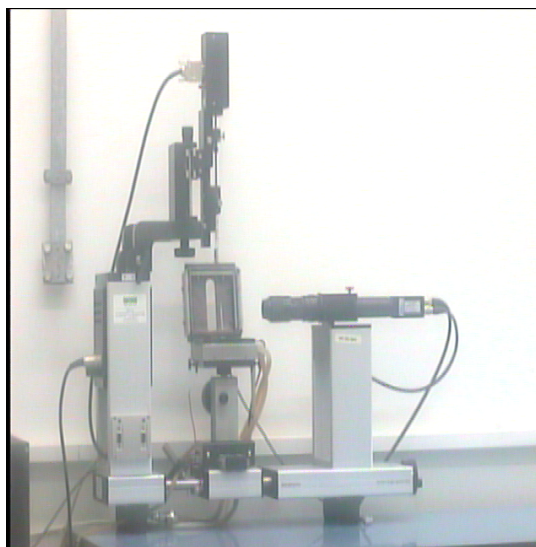


Figure 3-19: The tensiometer

The tensiometer is composed by:

A box (Figure 3-20) with a thermal regulated plate where the experimental cell is located, the box is free to translate in all three direction (x, y, z) for a correct positioning of the experimental cell (Figure 3-21).

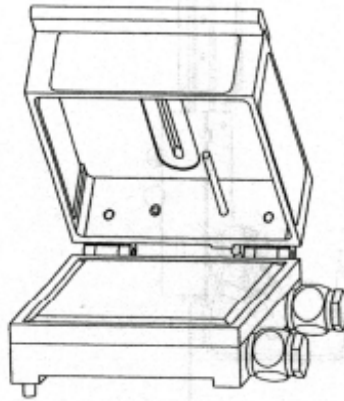


Figure 3-20: Thermal regulated box of tensiometer

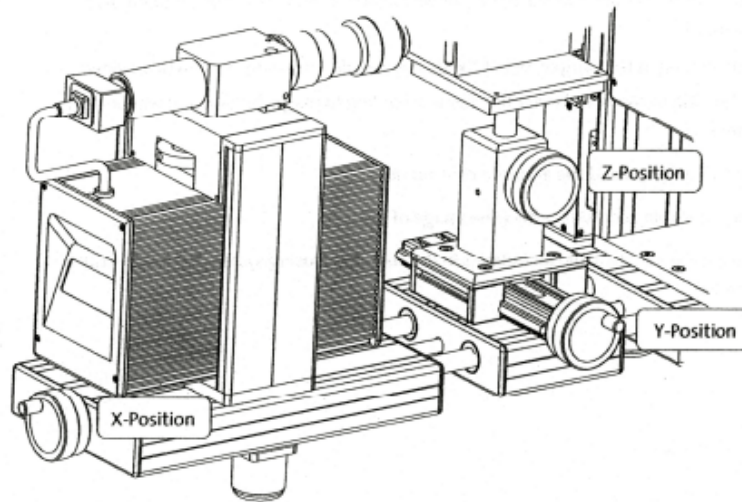


Figure 3-21: Controls for stage positioning

- A support for the injection system, with horizontal (Figure 3-22 B) and vertical (Figure 3-22 A) regulation.

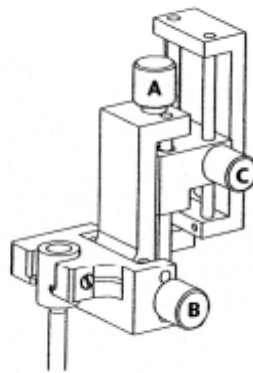


Figure 3-22: Controls for needle positioning

- The injection system with lodging for syringe (Figure 3-23). This system has an undercarriage for a precise dosing on the syringe piston. This undercarriage is commanded by the tensiometer software, for injection of highest precision: it's possible to inject a minimum volume of $0.007\mu\text{l}$ using a syringe Hamilton $500\mu\text{l}$ (Figure 3-24). Minimum and maximum dosing rate are respectively $0.06\ \mu\text{l/s}$ and $26.4\ \mu\text{l/s}$.

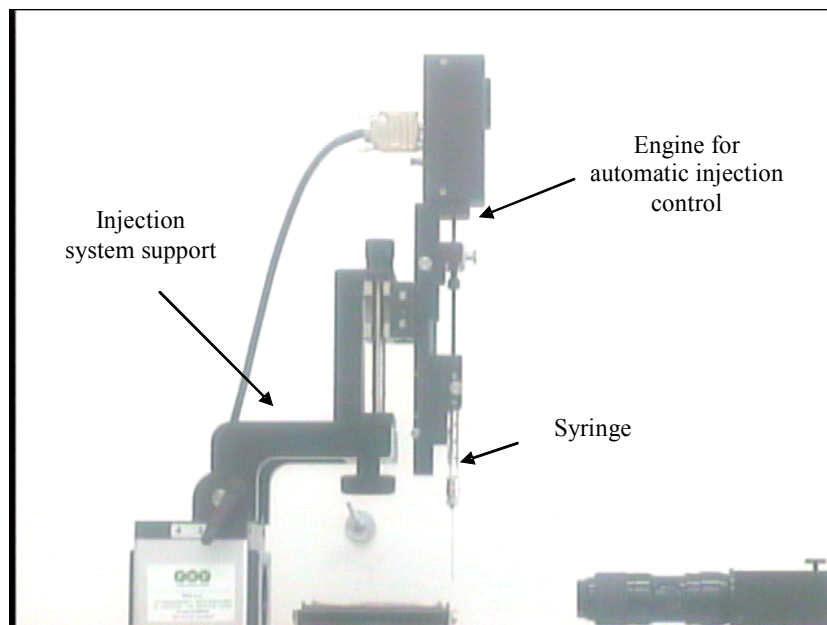


Figure 3-23: Injection system with automatic control

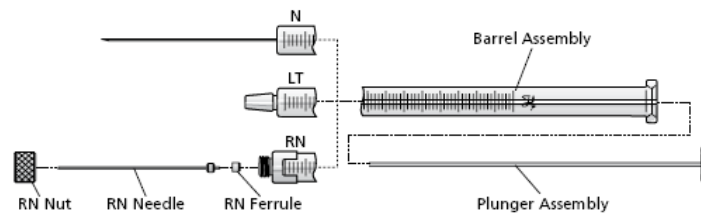


Figure 3-24: Scheme of Hamilton 500µl series 700 [23]

- Halogen lighting with continuously adjustable intensity without hysteresis for a homogeneous back lighting.
- Six-fold zoom lens (0.7 ... 4.5-fold magnification) with integrated fine focus (± 6 mm) and high light transmitting capacity CCD-camera (Figure 3-25) with a resolution of 752 x 582 pixels. Field of view (FOV): 1.31 x 1.05 ... 8.77 x 6.75 mm. Optical distortion: < 0.05 %



Figure 3-25: CCD camera

- Thermal control system of upper plate of thermal control box (see fig. III.2.3);
- Software “SCA 20” (Figure 3-26), for the surface tension measurements and for analysis. To run the software SCA 20 the PC must be able to run Windows NT 4.0, Windows 2000 or Windows XP without failure. In our case is a Pentium IV with 2.4GHz has been used with Windows 2000 service pack 3 and a ATI graphic Adapter XPERT 128 with a 3D Rage 128 Pro chip-set as recommended by operating manual of Dataphysics.

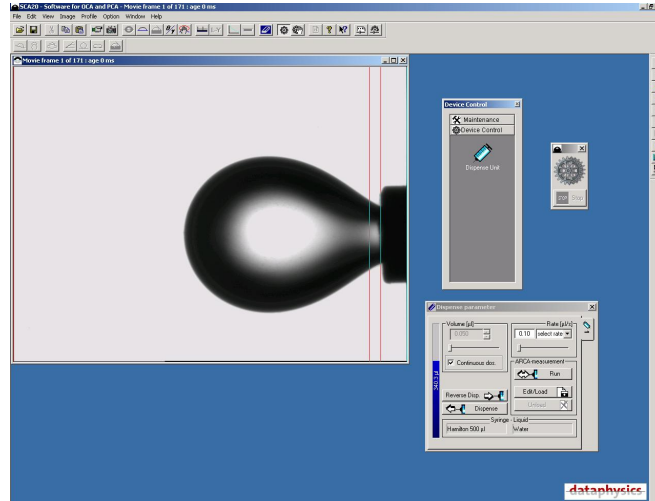


Figure 3-26: Graphic interface of SCA20 software control

A good quality of the drop image is very important for a correct surface tension measurement.

3.2.2 *Technique of measurement: Algorithm for surface tension measurements*

The measurement of surface tension of a liquid in its saturate vapour with the pendant drop technique is based on the solution of the Young-Laplace equation that binds the pressure drop through the liquid-vapour interface to the two main curvatures:

$$\Delta p = \sigma \left(\frac{1}{R_1} + \frac{1}{R_2} \right) \quad (3.1)$$

where: σ it is the surface tension

R_1 and R_2 are the two main curvature radii

$\Delta p = (p_1 - p_2)$ it is the pressure difference across the interface

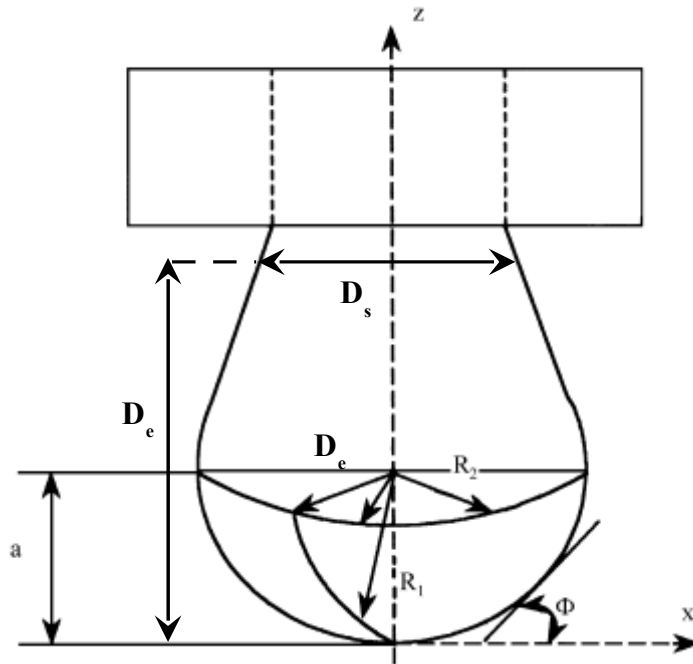


Figure 3-27: The pendant drop geometry

In presence of the terrestrial gravitational field, the hydrostatic pressure is given by well known Stevino law:

$$p = p_0 - \rho g z \quad (3.2)$$

where z is the distance, in vertical direction, measured from the apex of the drop.

The shape of a pendant drop is deformed with respect to the spherical one because the hydrostatic pressure is reduced as z increases in the liquid (while the variations in the surrounding gas are negligible). The pressure difference along the surface of the pendant drop increases downward extremity according to the Young-Laplace equation the curvature radius is reduced, an increment of main curvature. Replacing in the equation of Young-Laplace the Stevino equation one obtains:

$$p_{01} - p_{02} + \Delta \rho g z = \sigma \left(\frac{1}{R_1} + \frac{1}{R_2} \right) \quad (3.3)$$

where: $\Delta \rho = \rho_1 - \rho_2$ it is the density difference between the two phases.
 p_{01} and p_{02} are the pressures at the two sides of the interface in a reference point.

If the reference point is the drop apex, and if we assume that in this point $R_1=R_2=a$, then

$$p_{01} - p_{02} = \frac{2 \sigma}{a} \quad (3.4)$$

and the Young-Laplace equation (3.3) reads:

$$\Delta \rho g z + \frac{2 \sigma}{a} = \sigma \left(\frac{1}{R_1} + \frac{1}{R_2} \right) \quad (3.5)$$

if we consider the geometric relationships between R_1 , R_2 and x and z coordinates of drop profile [35]

$$z = z(x) \quad (3.6)$$

$$ds = \pm \sqrt{(dx)^2 + (dz)^2} \quad (3.7)$$

$$\phi = \arctan \left(\frac{dz}{dx} \right) \quad (3.8)$$

$$\frac{1}{R_1} = \frac{d\phi}{ds} = -\frac{d(\cos \phi)}{dz} = \frac{\frac{d^2 z}{dx^2}}{\left[1 + \left(\frac{dz}{dx} \right)^2 \right]^{\frac{3}{2}}} \quad (3.9)$$

$$\frac{1}{R_2} = \frac{\sin \phi}{x} = \frac{\frac{dz}{dx}}{x \left[1 + \left(\frac{dz}{dx} \right)^2 \right]^{\frac{1}{2}}} \quad (3.10)$$

then the Young-Laplace equation can be rewritten, according to Bashforth and Addams [36], through an equivalent differential equations system:

$$\frac{dx}{ds} = \cos \phi \quad (3.11)$$

$$\frac{dz}{ds} = \sin \phi \quad (3.12)$$

$$\Delta \rho g z + \frac{2\sigma}{a} = \sigma \left\{ \frac{\frac{d^2z}{dx^2}}{\left[1 + \left(\frac{dz}{dx} \right)^2 \right]^{\frac{3}{2}}} + \frac{\frac{dz}{dx}}{x \left[1 + \left(\frac{dz}{dx} \right)^2 \right]^{\frac{1}{2}}} \right\} \quad (3.13)$$

with boundary condition

$$x(0) = z(0) = \phi(0) = 0$$

$$\left. \frac{dx}{ds} \right|_{s=0} = 1 \quad \left. \frac{dz}{ds} \right|_{s=0} = 1 \quad \left. \frac{d\phi}{ds} \right|_{s=0} = \frac{1}{a}$$

where x and z are respectively the horizontal and vertical coordinates measured from the bottom point of the drop.

s is the curvilinear abscissa along the surface of the drop.

Φ is the angle between the tangent to the surface and the horizontal

a is the radius of curvature at the bottom of the drop.

If we consider (3.9) and (the 3.10), equation (3.13) it can be expressed also like

$$\frac{d\phi}{ds} = \frac{2}{a} + \frac{\Delta\rho g z}{\sigma} - \frac{\sin\phi}{x} \quad (3.14)$$

therefore, if all lengths of the equation are dimensionless with respect to **a**, the equation becomes

$$\frac{d\phi}{ds^*} = 2 + \beta z^* - \frac{\sin\phi}{x^*}$$

where the only parameter β , is defined as:

$$\beta = \frac{\Delta\rho g a^2}{\sigma}$$

β is the Bond number, measuring the ratio between the gravitational forces and the surface tension forces and is the responsible factor of the shape of the drop. When the Bond number is close to zero, surface tension effects prevail and the drop becomes almost spherical, while for relatively high Bond number, the drop assumes the typical shape lengthened by the gravity effect.

For the evaluation of the surface tension the theoretical shape of drop must be compared with the experimental fitting carried out by the software tensiometer: from this comparison it's possible to evaluate the values of β and **a**. At this point the surface tension is computed as:

$$\sigma = \frac{\Delta\rho g a^2}{\beta} \quad (3.15)$$

In 1882, Bashforth and Adams derived the theoretical form of a pendant drop and calculated tables of drop contours. The tables can be used to determine the surface tension by fitting the experimentally measured drop contour to the theoretical curve. However, this procedure is very tedious. To simplify this procedure, the following empirical relationship was proposed by Andreas [37]

$$\sigma = \frac{g D_e^2 \Delta \rho}{H}$$

where D_e is the equatorial diameter of drop

H is a correction factor which is related to the shape factor of the pendant drop, S , defined as:

$$S = \frac{D_s}{D_e}$$

where D_s is the drop diameter measured horizontally at a distance D_e away from apex of the drop (Figure 3-27).

The analysis process, carried out by the software of the tensiometer, consists of three steps:

- 1) Capture and digitalization of the image of the pendant drop
- 2) Extraction of the drop contour, determination of the radius of curvature at the apex necessary for the calculation of surface tension;
- 3) Shape comparison between the theoretical and experimental drop, inferring the surface tension value.

These three steps are described below:

- 1) The drop is captured by the frame grabber with a resolution of 582x752 square pixels using software tools of the tensiometer.
- 2) An edge detection program is used after the digitization of the image of the drop to obtain its contour. The contour of the drop is defined by the last pixel with a grey level higher than the threshold value. Some researchers [38] have shown that the surface tension value is affected by less than 1% if the contour of the drop is chosen based on the last black (above threshold) instead of the first white (below the threshold) pixel. For to evaluate the correct surface tension measurement is necessary to know the radius of curvature at the apex of the drop. This radius is taken as the distance between the apex and the centre of the diameter, as shown in Figure 3-28a. In the case of longer drops, as shown in Figure 3-28b, the

values of the radius at the apex are overestimated then in this case circles of different radii are superposed to the maximum number of points around the apex. The radius of the circle that superposes to maximum number of points is taken equal as the radius of curvature of the drop at the apex.

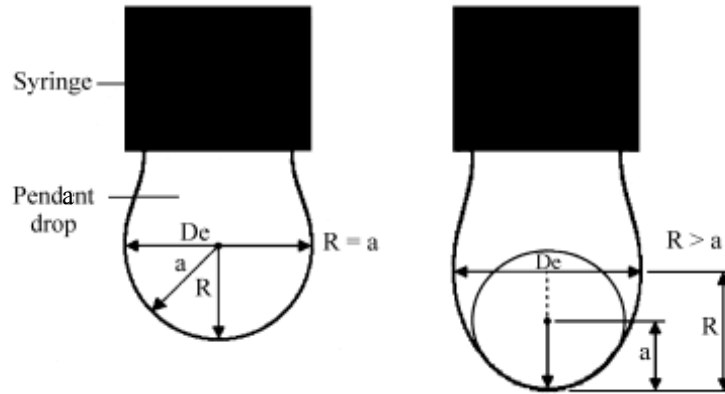


Figure 3-28: Evaluation of the radius of curvature at the apex of drop

- 3) The software of the tensiometer makes a comparison of the shapes using the experimental points after smoothing and the theoretical point found by solving the Bashforth and Adams equation. This equation is first solved for a value of β approximated by the empirical formula of Huh and Reed [39]:

$$\beta = \sqrt{\exp(-6.70905 + 15.30025 S - 16.44709 S^2 + 9.92425 S^3 - 2.585035 S^4)}$$

The comparison is operated diminishing the standard deviation between the experimental and numerical values of four parameters: \mathbf{a} , β and the coordinates in pixel of the apex of the drop \mathbf{x}_0 and \mathbf{z}_0 . While the value of standard deviation is major of target value fixed, β is increased, until it is minor then a fixed value: so the iteration is finished and the last value of β is the optimal value.

Replacing in the 3.15 the β and \mathbf{a} values it's possible to evaluate the surface tension.

3.2.3 Measurements results

In order to measure a correct value of surface tension of mixtures studied, it has been necessary to do a calibration of experimental setup. In Figure 3-29 has been shown the comparison between the experimental results and literature values for two different liquids, water for pure liquid and water-heptanol solution at concentration of 0.1 weight percentage (w%): results are in good agreement with literature value.

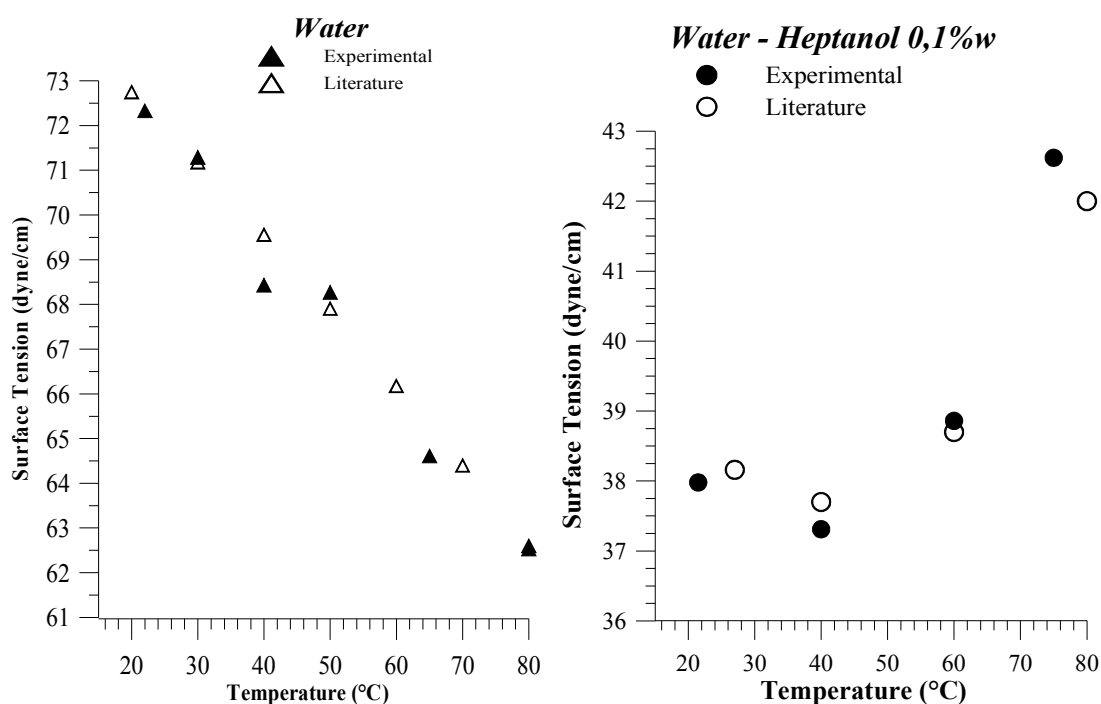


Figure 3-29: Calibration of experimental setup with water and water-heptanol solutions

As shown in the Figure 3-29 all measurements have been performed in the range of 20-80°C, the solutions investigated have been firstly two different alcoholic solution, water-based, at different concentration to study the effect of concentration on the dependency of surface tension with temperature and concentration.

Below (Figure 3-30) are shown the results for a solution of water-butanol at concentration of 1-5-7w% and for water-heptanol at concentration of 0.1 and 0.2w%.

In Figure 3-30 is also possible to note the surfactant behaviour of alcohol in water base solution, in fact when the concentration reaches the solubility value the surface tension measurement is very close to the surface tension of pure alcohol. This happens because, like a surfactant, alcohol molecules are distributed on the liquid-air interface

saturating the surface, in others term we can assume that at the solubility concentration the composition of the surface are rich in alcohols so that also the surface tension is close to the pure alcohol.

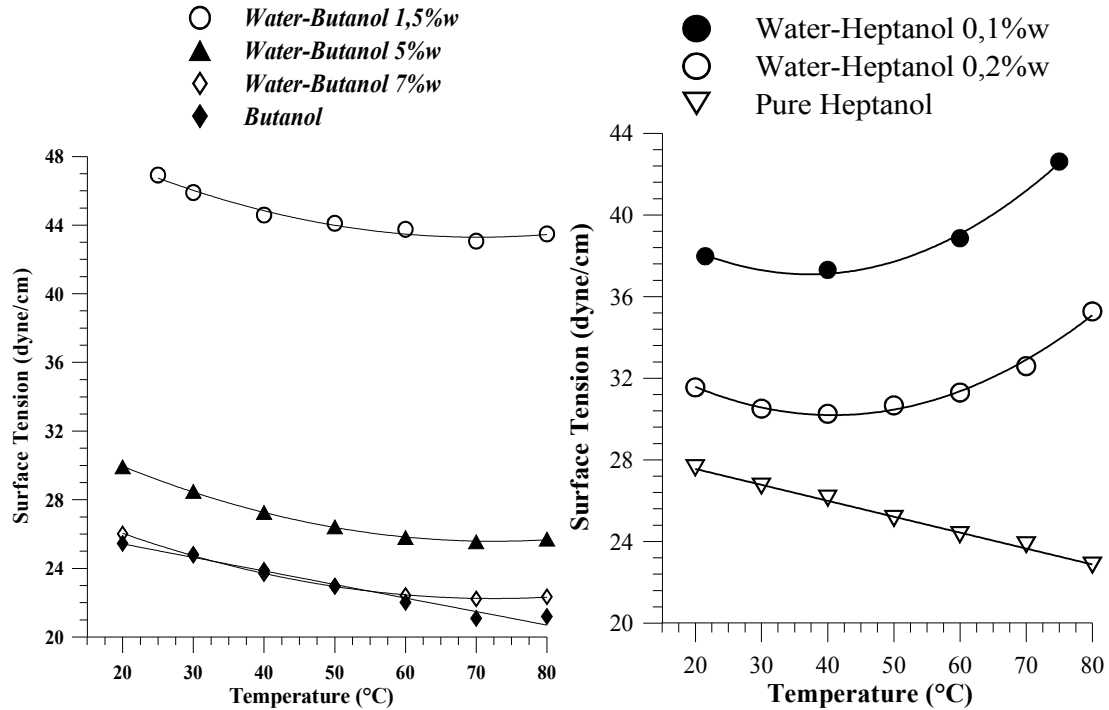


Figure 3-30: Effect of concentration of alcohol in water-butanol and water-heptanol solutions

In particular for space application two different commercial brine (solutions with a low freezing point) have been selected as possible working fluid for space heat pipe: FP40 (a mixture of water and potassium formate) and FD40 (mixture of potassium hydroxide, acetic acid and water). In order to realize a self rewetting brine also in this case has been added a little amount of alcohol to the based mixture.

Figure 3-31 shows that the addition of alcohol gives a self-rewetting behaviour to the based brine, in particular in comparison with water-based mixture the temperature of the minimum point of surface tension is lower. Table 3-5 resumes the results in term of surface tension derivative at each temperature range.

Self-Rewetting Solutions & Brines

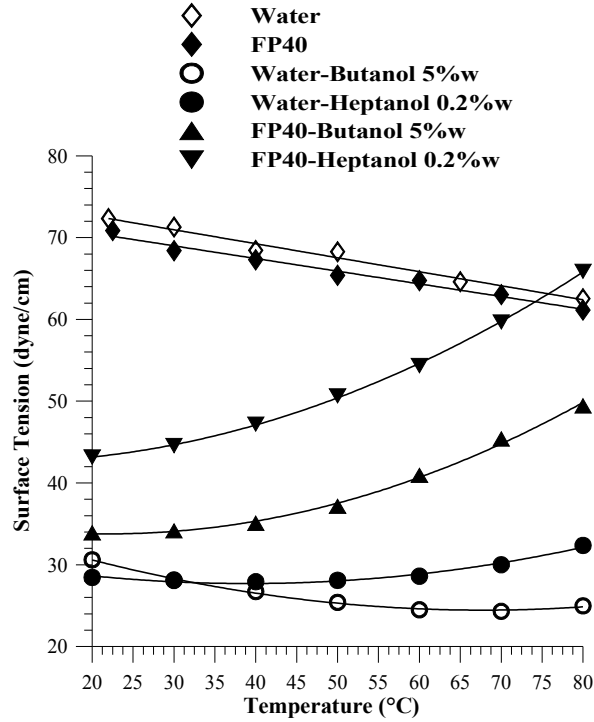


Figure 3-31: Surface tension measurements of FP40 and FD40 and self-rewetting brines

Solutions	σ_T at 20°C	σ_T at 40°C	σ_T at 60°C	σ_T at 80°C
Water -Butanol 5%w	-0.247	-0.137	-0.055	0.067
Water-Heptanol 0.2%w	-0.037	0.001	0.096	0.236
FP_40-Butanol 5%w	0.025	0.150	0.382	0.452
FP_40-Heptanol 0.2%w	0.141	0.305	0.452	0.620

Table 3-5: Comparison in term of surface tension derivative with temperature of self-rewetting fluids and self-rewetting brines

After characterization of self-rewetting fluids and brines, in collaborations with Utsonomya University, MIT and ENEA have been produced several self-rewetting fluids based on nanofluids. In Figure 3-32 are shown the results obtained for four silver-capped nanofluids with additcion of butanol at concentration of 5w%.

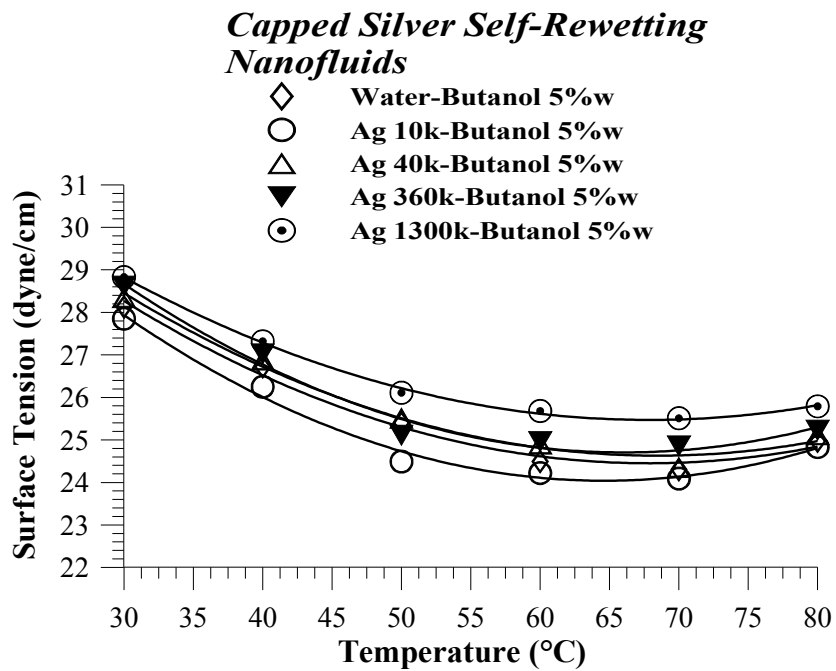


Figure 3-32: Surface tension measurements of self-rewetting silver nanofluids

The results show that there are not any change in term of surface tension values and surface tension derivative with temperature respect the base self-rewetting fluids (Water-butanol 5w%), also in this case we can find that the addiction of alcohol produce an self-rewetting behaviour on the base-mixture. The same results have been found on the self-rewetting nanohorn Figure 3-33 (discussed in second chapter of this work).

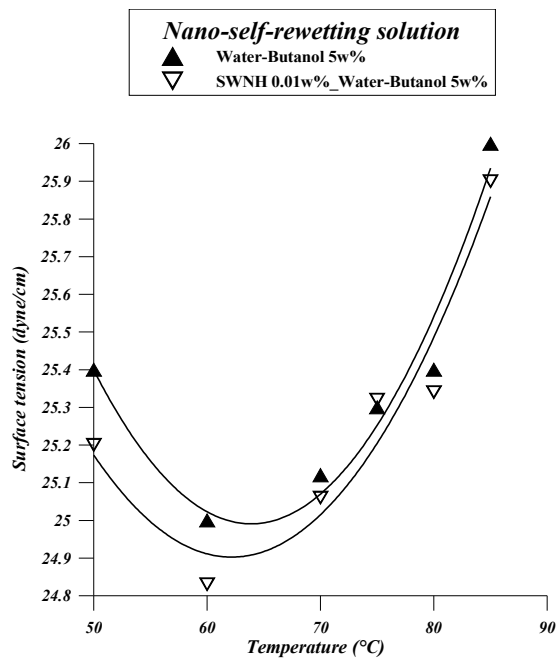


Figure 3-33: Surface tension measurements of self-rewetting nanofluids based on SWNH

3.3 Contact Angle measurements

3.3.1 Technique of measurement

For the contact angle measurements it have been utilized the contact angle meter OCA15+, it's the same instrument which has been utilized for surface tension measurement. Next are described the various techniques of measurement.

All calculation methods are based on the sessile drop method, i.e. drops of liquid are deposited on a solid surface (as smooth and horizontal as possible).

A distinction has to be made between the various ways of measuring the drop:

- A contact angle can be measured on static drops. The drop is produced before the measurement and has a constant volume during the measurement.

- A contact angle can be measured on dynamic drops. The contact angle is measured while the drop is being enlarged or reduced; the boundary surface is being constantly newly formed during the measurement. Contact angles measured on increasing drops are known as “advancing angles”; those measured on reducing drops as “retreating angles”.

Clearly, in a static contact angle measurement, the size of the drop does not change during the measurement. However, this does not mean that the contact angle always remains constant; on the contrary, interactions at the boundary surface can cause the contact angle to change considerably in time. Depending on the type of time effect, the contact angle can increase or decrease during the observation.

For example, these interactions could be:

- Evaporation of the liquid
- Migration of surfactants from the solid surface to the liquid surface
- Substances dissolved in the drop migrating to the surface (or in the opposite direction),
- Chemical reactions between the solid and liquid,
- The solid being dissolved or swollen by the liquid.

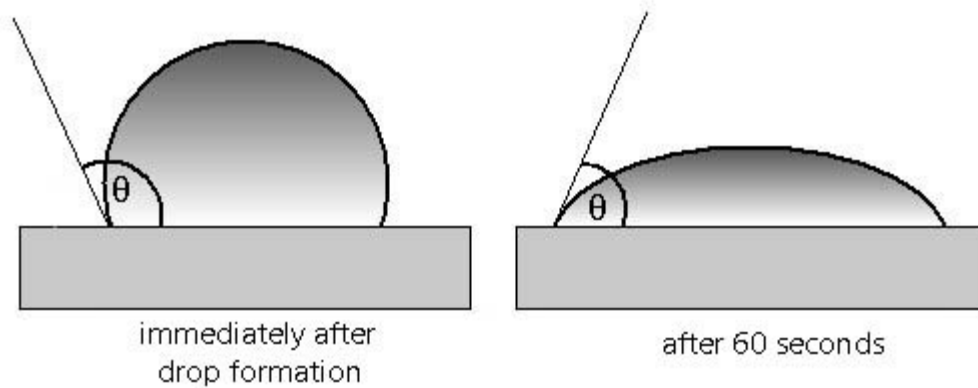


Figure 3-34: Alteration of the static contact angle as function of time

It may be a good idea to choose to measure the static contact angle when its variation as a function of time is to be studied. A further advantage of static contact angle measurement is that the needle does not remain inside the drop during the measurement. This prevents the drop from being distorted (particularly important for small drops). In addition, when determining the contact angle from the image of the drop it is possible to use methods which evaluate the whole drop shape and not just the contact area.

Certain materials which don't show a fully rigid surface (e.g. rubber) are better being tested with static measurements. In such cases, dynamic contact angles are poorly reproducible.

However, changes with time often interfere with the measurement. There is also another source of error: as the static contact angle is always measured at the same spot on the sample any local irregularities (dirt, inhomogeneous surface) will have a negative effect on the accuracy of the measurement. On the contrary, this error can be averaged out in dynamic one.

The dynamic contact angle is an outcome of the processes at the liquid/solid boundary during the increase in volume (advancing angle) or decrease in volume (retreating angle) of the drop, i.e. during the wetting and dewetting processes.

A boundary is not formed instantaneously but requires some time before a dynamic equilibrium is established. This is why a flow rate which is too high should not be selected for measuring advancing and retreating angles, as otherwise the contact angle will be measured at a boundary which has not been completely formed. However, it should also not be too slow as the time effects mentioned above will then again play a

role. In practice flow rates between 5 and 15 ml/min are recommended; higher flow rates should only be used for the simulation of dynamic processes. For high-viscosity liquids (e.g. glycerol) the rate will tend to approach the lower limit.

The basis for the determination of the contact angle is the image of the drop on the drop surface. In the SCA20 program the actual drop shape and the contact line (baseline) with the solid are first determined by the analysis of the grey level values of the image pixels. More precisely, the software calculates the root of the secondary derivative of the brightness levels to receive the point of greatest changes of brightness. The found drop shape is adapted to fit a mathematical model which is then used to calculate the contact angle. The various methods of calculating the contact angle differ therefore in the mathematical model used for analyzing the drop shape or only part of it. All methods calculate the contact angle as tang at the intersection of the drop contour line with the solid surface line (base line). In the following sections the different drop shape analysis methods are briefly described.

Tangent method 1

The complete profile of a sessile drop is adapted to fit a general conic section equation. The derivative of this equation at the intersection point of the contour line with the baseline gives the slope at the 3-phase contact point and therefore the contact angle. If dynamic contact angles are to be measured, this method should only be used when the drop shape is not distorted too much by the needle.

Tangent method 2

That part of the profile of a sessile drop which lies near the baseline is adapted to fit a polynomial function of the type $(y=a + bx + cx^{0.5} + d/\lnx + e/x^2)$. The slope at the 3-phase contact point at the baseline and from it the contact angle are determined using the iteratively adapted parameters.

This function is the result of numerous theoretical simulations. The method is mathematically accurate, but is sensitive to distortions in the phase contact area caused by contaminants or surface irregularities at the sample surface.

As only the contact area is evaluated, this method is also suitable for dynamic contact angles. Nevertheless, this method requires an excellent image quality, especially in the region of the phase contact point.

Height-width method

In this method the height and width of the drop shape are determined. If the contour line enclosed by a rectangle is regarded as being a segment of a circle, then the contact angle can be calculated from the height-width relationship of the enclosing rectangle. The smaller drop volume, the more similar is the shape of the drop to the theoretically assumed spherical cap form. As the drop height cannot be determined accurately when the needle is still in the drop, the height-width method is not suitable for dynamic drops. This method also has the disadvantage that the drops are regarded as being symmetrical, so that the same contact angle is obtained for both sides, even when differences between the two sides can be seen in the actual drop image.

Circle fitting method

As in the height-width method, in this method the drop contour is also fitted to a segment of a circle. However, the contact angle is not calculated by using the enclosing rectangle, but by fitting the contour to a circular segment function. The same conditions apply to the use of this method as to the height-width method with the difference that a needle remaining in the drop disturbs the result far less.

Young-Laplace (sessile drop fitting)

The most complicated, but also the theoretically most exact method for calculating the contact angle is the YOUNG-LAPLACE fitting. In this method the complete drop contour is evaluated; the contour fitting includes a correction which takes into account the fact that it is not just interfacial effects which produce the drop shape, but that the drop is also distorted by the weight of the liquid it contains. After the successful fitting of the YOUNG-LAPLACE Equation the contact angle is determined as the slope of the contour line at the 3-phase contact point.

If the magnification scale of the drop image is known (determined by using the syringe needle in the image) then the interfacial tension can also be determined; however, the calculation is only reliable for contact angles above 30°. Moreover, this model assumes a symmetric drop shape. Therefore it cannot be used for dynamic contact angles where the needle remains in the drop.

It has been chosen to make the static contact angle measurement utilizing the last method because is certainly the slowest and the most accurate method of contact angle measurement.

Below it's shown a picture of a pure water drop on the aluminium surface. Many parameters influences a contact angle measurement, the more relevant are:

- Quality of test liquid
- Time
- Temperature
- Volume
- Density
- Gravitation
- Quality of the surface
- Preparation of the surface
- Dosing rate
- Drop size
- Drop environment
- Evaporation
- Adsorption and absorption
- Partial soluble surface

For this reasons has been defined the standard condition for the experimental measurement: the drop should be as small as possible and the fitting and the measurement is carried out after five second by injection, because there is not a consistent evaporation of test liquid and a significant changing of sessile drop shape.

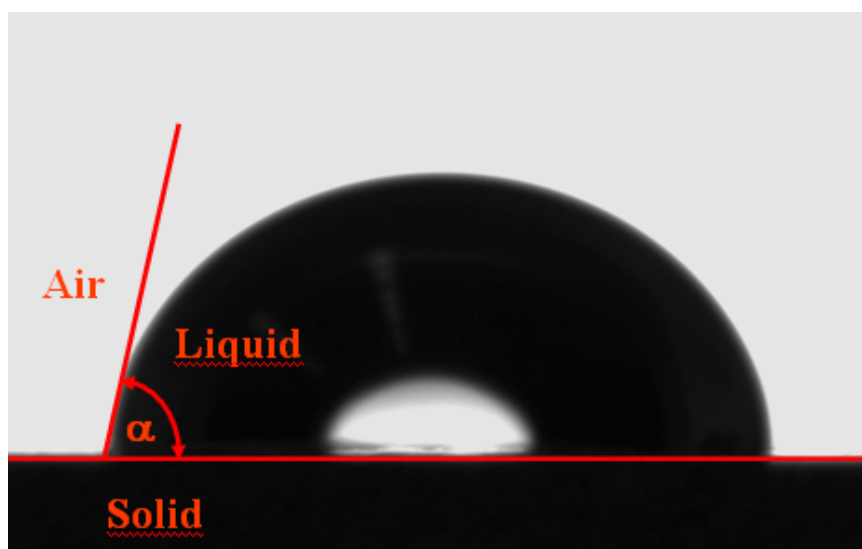


Figure 3-35: A sessile pure water drop on aluminium surface

3.3.2 Measurements results

Two different surface have been chosen, copper and aluminium surface; in Table 3-6 are listed the results of different liquids in particular pure water as conventional working fluids and self-wetting fluids as binary mixture and self-wetting brines and nano-self-wetting fluids as ternary mixture a nanofluids. The main result is about the effect of alcohol in the base solution: in fact when a little amount of alcohol is added to base fluid it is possible to observe a great decreasing of contact angle. This result is very important related to the effect of contact angle on the capillary pressure, a better wettability produce a great increasing of capillary pressure and can bring to an higher critical heat flux for self-wetting solution in comparison with conventional fluids as it will be shown in the next chapters.

<i>Fluid</i>	<i>Copper (Cu)</i>	<i>Aluminium (Al)</i>
Water	82°	82°
FP40	90°	89°
Heptanol	12°	7°
Butanol	10°	6°
Water- 0.2% Heptanol	59°	56°
Water- 5% Butanol	54°	51°
FP40- 0.2% Heptanol	76°	75°
FP40- 5% Butanol	67°	64°
Water – 5% Butanol - Nanohorn	53°	51°

Table 3-6: Contact angle measurements of copper and aluminium surface

3.4 Thermal conductivity measurements

3.4.1 Experimental Setup and Measurement Technique

In this work has been utilized an home-made apparatus for the thermal conductivity measurements based on the parallel plate steady-state technique. In steady-state techniques such as the parallel plate [40] and coaxial cylinder methods [41], heat is transferred between two plates (or coaxial cylinders) sandwiching the test fluid. Measurement of the temperature difference and heat transfer rate across the fluid can be used to determine the thermal conductivity via Fourier's law.

$$k = \frac{Q/A}{\Delta T/\Delta L}$$

Where Q is the heat flux measured, A is the surface of the copper plate, ΔT is the difference of temperature between the sides of the liquid bridge and ΔL is the thickness of the liquid bridge or the distance between the copper rods.

A liquid layer is formed between two copper rods with 2 cm diameter. Four thin thermocouples (K-type) located above and below the sample were soldered into the copper bars at different axial locations (Figure 3-36). Thin foil fluximeters are installed inside the copper rods to measure the heat flux, this can be measured through an opportune calibration constant and the difference of temperature between two sides of kapton fluximeter.

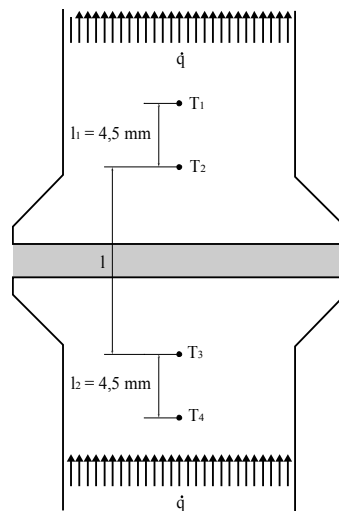


Figure 3-36: : Scheme of parallel plate apparatus to measure the thermal conductivity

When the steady state condition occurs it is possible to do a thermal conductivity measurements, as just described. In order to avoid the problem related to measure with extremely precision the liquid thickness and the rods' surface area, it has been preferred to not perform an absolute measurement of thermal conductivity but a relative measurement, because of this all measurements will be reported as ratio between the thermal conductivity of sample and a reference liquid (pure water in this case). This artifice simplify a lot the measurement, in fact it is necessary just to measure the difference of temperature of fluximeter and the sample liquid bridge, and make a ratio between the results of measurement for the sample and the reference liquid. The

necessary hypothesis is that the distance between two rods has fixed and not change during the measurements of several liquids.

$$\frac{K_s}{K_w} = \frac{Q_s}{Q_w} \frac{\Delta T_w}{\Delta T_s}$$

Where with subscript **s** has been indicated the sample and with **w** the water.

3.4.2 Measurements Results

Nearly 10 measurements have been done for all samples measured. The solution measured in this work are the self-wetting fluids base on water and on FP40 , two nanofluids manufactured by MIT (gold and silica), the silver capped nanofluids and self-wetting carbon nanofluid that have already been considered in previous discussion. In particular for the last solution three different concentrations of the carbon nanohorns have been dispersed in water-butanol mixture at the concentration of 5w%.

In Table 3-7 has shown the results relative of all fluid studied without the results of self-wetting nanohorns that will be shown below and discussed separately to first class of fluid and nonofluids.

<i>Solutions</i>	<i>K/K_w</i>
Water-Butanol 5% w	0.91 – 0.92
Water-Heptanol 0.2% w	0.98 – 0.99
FP40-Butanol	0.69 – 0.70
Gold MIT	1.00 – 1.01
Silica MIT	1.13 – 1.15
A Silver Utsunomiya	1.01 – 1.03
B Silver Utsunomiya	1.00 – 1.02
C Silver Utsunomiya	0.99 – 1.01

Table 3-7: Thermal conductivity measurements of several liquids

As expected the thermal conductivity of self-wetting fluid composed by water and alcohol have a lower thermal conductivity than water, in fact the thermal conductivity of pure alcohol is three times lower than water and the measurements of the mixture depends on the concentration of alcohol. The same analysis it is possible to do about the mixture of FP40 and butanol, in fact both the thermal conductivity of brines and alcohols are lower than water.

No enhanced of thermal conductivity has been found for silver capped nanofluids and gold nanofluid, probably due to the very low concentration of nanoparticles in base

fluid; good enhanced of thermal conductivity instead has been found for silica nanofluids, in this case the concentration should be very high, many results in literature reporting a good increasing of thermal conductivity in the case of silica nanofluids with a concentration of nanoparticles around 20-30%w.

In order to characterize the behaviour of thermal conductivity of self-rewetting nanofluids based on nanohorn three different mixture have been prepared and measured, the results are shown in Figure 3-37.

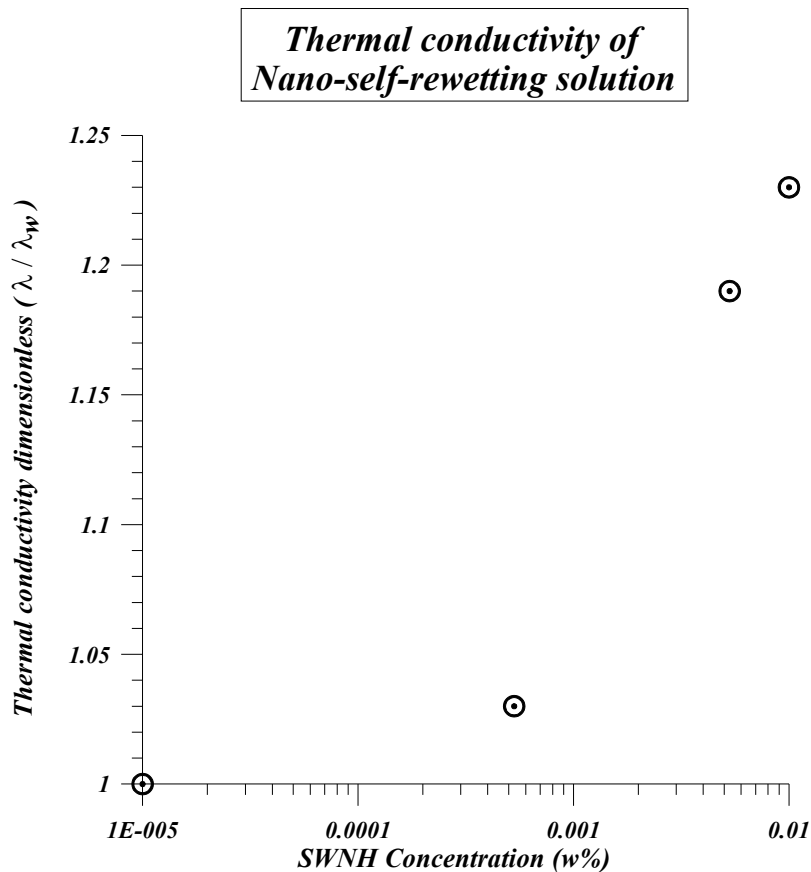


Figure 3-37: : Thermal conductivity measurements of “Nano-self-rewetting” solution based on dilute aqueous solution of butanol, dimensionless with thermal conductivity of pure water

These solutions, at three different concentrations of SWNH particles, have shown, in all cases, an higher thermal conductivity than relative base solutions. In particular very low amounts of SWNH (< 0.01 w%) are needed to achieve remarkable improvements in thermal conductivity (about 25% respect thermal conductivity of pure water). For these samples thermal conductivity increases with increasing concentration of SWNH in the range of concentrations investigated. These results could be correlated

to the peculiar structure of SWNH. In fact this material is mainly constituted by rolled and tangled graphene sheets, which are at the base of graphite structure. As known, thermal conductivity in graphene is highly in excess respect to those measured for carbon nanotubes and diamond. The presence of this peculiar crystalline structure instead of an amorphous one and the low dimensions of SWNH which enhances its capacity of being dispersed in a liquid medium are probably at the basis of the promising results obtained in thermal conductivity measurements.

4 Filling procedure and thermal tests of commercial heat pipes

4.1 Introduction

After the characterization of different mixtures, measuring the thermo-physical properties as discussed in previous chapter, the next step is related to perform thermal test with commercial heat pipe. The effect of filling ratio (defined as the ratio between the liquid volume in the heat pipe on the entire volume of its) will be studied together with the possible benefits of using a self-rewetting solution as new working fluids in heat pipe.

In order to do these kind of tests, a breadboard has been manufactured in DIAS laboratory, the specifics of this are the possibility to heat the heat pipe on a side (evaporator section) in order to avoid the heat loss during the test, to create a condenser region and to evaluate the temperature distribution along the pipe.

In Table 4-8 are reported the characteristics of heat pipe tested.

External diameter	0.800 cm
Thickness of wall	0,055 cm
Length	24,0 cm
Internal Volume	8.974 cm ³

Table 4-8: geometrical dimension of commercial heat pipe

Each test has been performed in horizontal condition in order to minimize the effect of gravity on the operative cycle.

The wick structure utilized in this experiment is a groove structure, each channel have a trapezoidal geometry with the dimension of 300 μ m-160 μ m for maximum and minimum base of trapeze with a high of 230 μ m.

Before passing to next paragraph it is necessary to define a very important parameter that all companies use in order to compare the thermal performances of heat pipe, the thermal resistance (TR). TR is so defined:

$$TR = \Delta T / Q$$

where ΔT is the difference of temperature between the evaporation section and condensation section and Q is the heat power supply, a low value of this parameter (<1) means that heat pipe work well, in general we can say that when the dry-out condition occurs the thermal resistance increase with the power heat supplied. In general, will be more clear below, the good range of operation for an heat pipe is when the thermal resistance is almost constant before the rising of this parameter.

4.2 Breadboard for Experimental Setup

The breadboard is composed by an aluminium structure, with a teflon cover in order to give a thermal insulating surface for allocation of heat pipes. They are allocated in Plexiglas blocks, where it is allocated the evaporator (Figure 4-38).

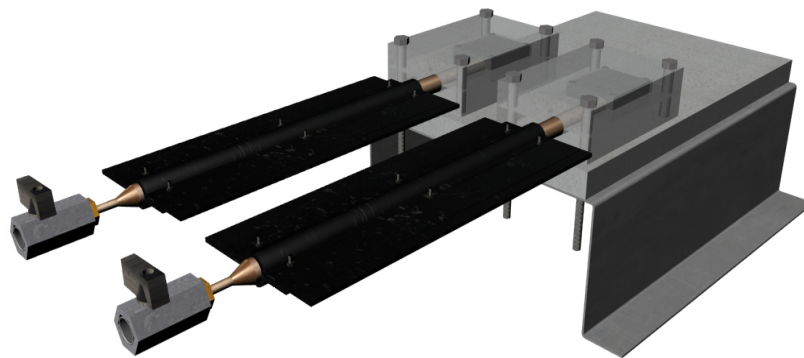


Figure 4-38: CAD rendering of breadboard

The last one is composed by an aluminium block with two holes: one is a passing holes, necessary to put the tube heat pipe, and the second one is not passing and it is need for allocation of a cartridge heater, supplied with a DC power supply.

The condenser is instead composed by two radiating aluminium plate (black painted) modelled with the shape of heat pipe tube, in Figure 4-39 a view of all parts of heat pipe allocation.

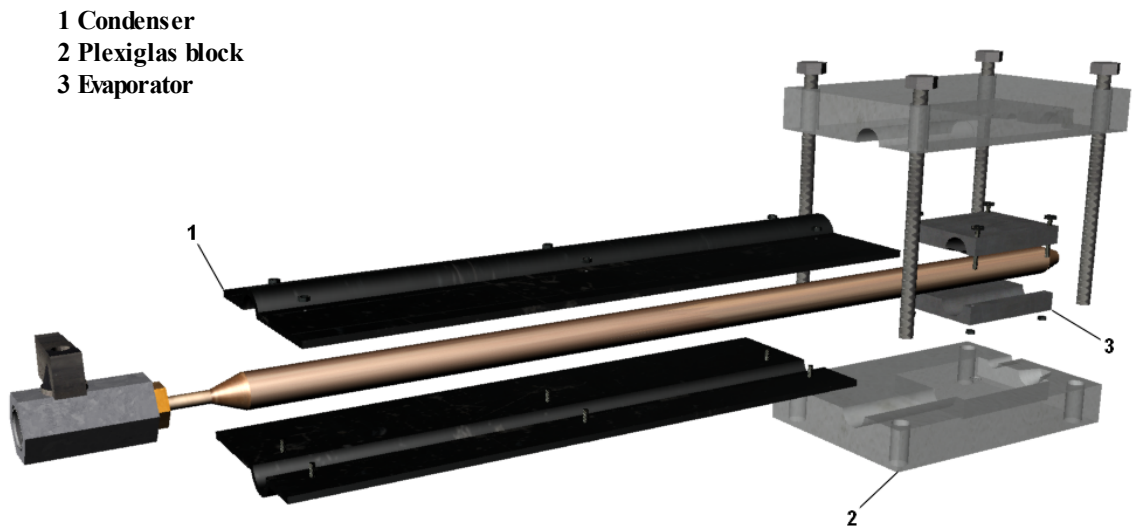


Figure 4-39: Explotted view of apparatus

The temperature evolution and distribution along heat pipe has been measured with 4 “K” thermocouples, each temperature signal has been acquired with a Data Logger.

Below each subsystem will be introduced in details.

In order to have the possibility to fill the heat pipe with different working fluids, a valve has been soldered (Figure 4-40) and tested in order to guarantee a perfect sealing during the tests. During the filling procedure that will be shown it has been needed to use a vacuum pump BOC Edwards XDS10, shown in Figure 4-41, and a cryostatic bath.

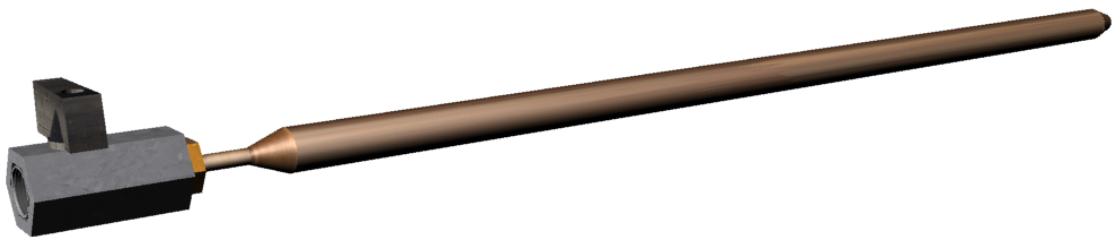


Figure 4-40: Detail of heat pipe with vacuum valve



Figure 4-41: Vacuum Pump BOC Edwards XDS10

In Figure 4-42 has been shown a CAD view of evaporator, the details of this subsystem is self-explained by the figure, the choice about the selection of aluminium as material is due to the fact that it have an extraordinary high thermal conductivity (401 W/mK) in order to not dissipate the energy given by cartridge heater.

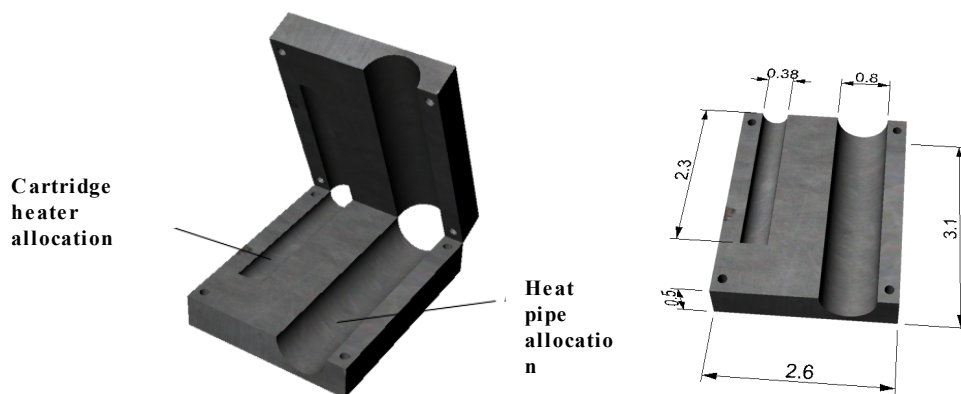


Figure 4-42: 3D Evaporator view and section

As just discussed before the condensator has been realized with two thin aluminium plates (Figure 4-43), black painted having and relative emissivity coefficient near to 1 necessary for having the best heat exchange possible.



Figure 4-43: Condensator (3d CAD quotation view)

A scheme of cartridge heater that has been utilized for supply heat to the evaporator has been shown in Figure 4-44: core of the device is the Nickel-Chrome resistance wire that is necessary to convert the electrical power in heat power through Joule Effect, the lead wire will be connect to power supply.

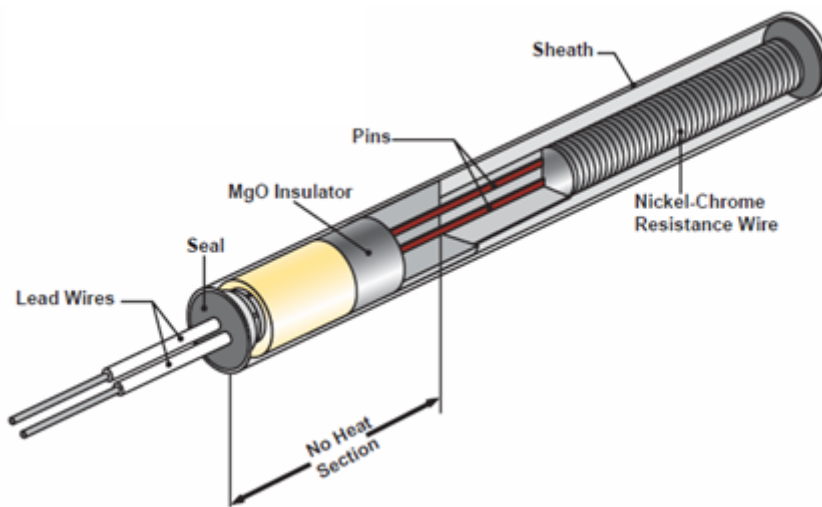


Figure 4-44- Scheme of cartridge heater

Four thermocouples are located as shown in Figure 4-45, in order to measure the thermal resistance of heat pipe and check the goodness of filling procedure, and are acquired with Multichannel Integra 2701 Keithley instruments, are acquired (Figure 4-46). This system can acquire a maximum of 20 channels with a maximum data rate of 3500 dps (data per second)

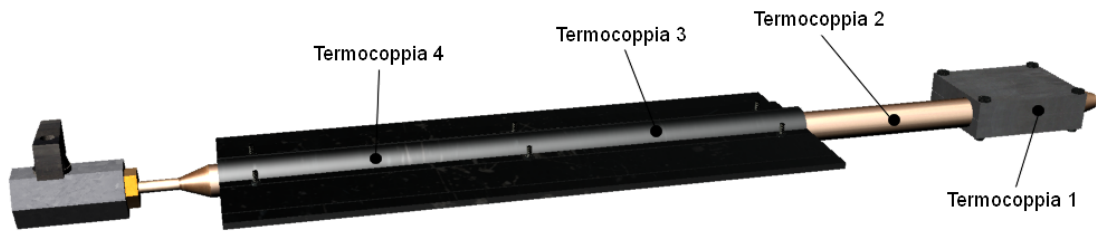


Figure 4-45: Thermocouples location



Figure 4-46: Data Logger

4.3 Filling procedure

This is the most critical part of the thermal test: the necessity to do a filling procedure born by the fact that it is absolutely important that in the heat pipe there is the liquid in equilibrium with his vapour, without air and without non-condensable gas. All steps that will be described have been made in order to prevent these problems and to have a good repeatability of results.

The filling procedure has been named IDT (Icing Degassing Technique) and it consist in the follow steps:

1. Filling of heat pipe with the amount of liquid necessary
2. The heat pipe is immersed in a cryostatic bath at the temperature of approximately -20°C for ~ 30 minutes for favour the icing process of the liquid (Figure 4-47).
3. Vacuum is realized in the inner of the pipe, through opening/closing of A valve (Figure 4-47).

4. With a insulated copper wire connected with a power supply, the heat pipe is heated in entire length with a constant temperature around 130°C: with this procedure all non-condensable gases are released in vapor phase (Figure 4-48).

5. In order to evacuate the non-condensable gases from heat pipe, the point 2 is repeated.

After IDT procedure the heat pipe is weighed in order to estimate the amount of liquid in the heat pipe, then the filling ratio.

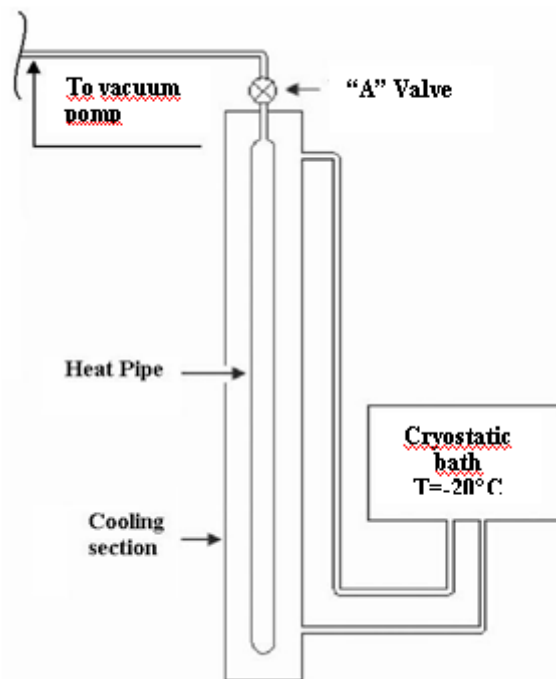


Figure 4-47: scheme for resuming 2-3 steps of IDT procedure

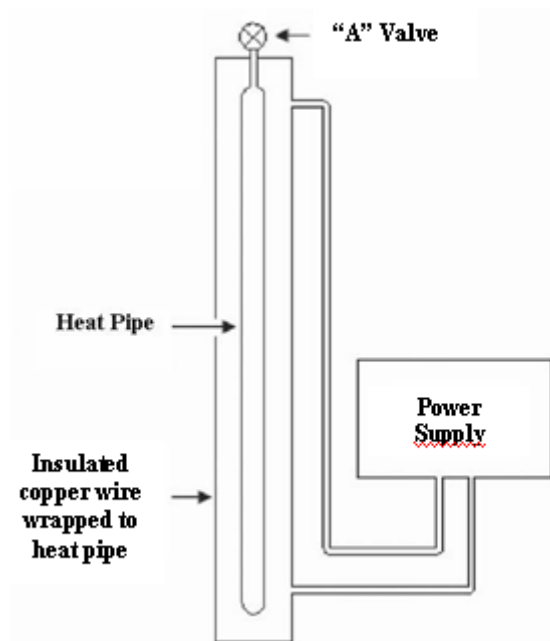


Figure 4-48: scheme for resuming 4 step of IDT procedure

4.4 Results

4.4.1 Objectives

The thermal test has been performed in all cases in horizontal configuration for the following purposes:

- Comparison between three different working fluids for the filling of the groove commercial heat pipe with a filling ratio of 25% (commonly utilized in commercial heat pipe)
- Theoretical and experimental results on effect of filling ratio with pure water as working fluid
- Introduction of a fan in the experimental setup for simulation of a dummy cpu
- Comparison between pure water and self-wetting fluids with new configuration of experimental setup

4.4.2 Pure Water, Self-rewetting and Self-rewetting nanofluids as working fluid in a commercial groove heat pipe

As just discussed before a commercial heat pipe has been filled with three different working fluids in order to estimate the differences in term of thermal resistance and maximum temperature of the evaporator. In Figure 4-49 and Figure 4-50 are shown the results utilizing pure water, a mixture of water-butanol 5w% and the same last mixture with a dispersion of SWNH.

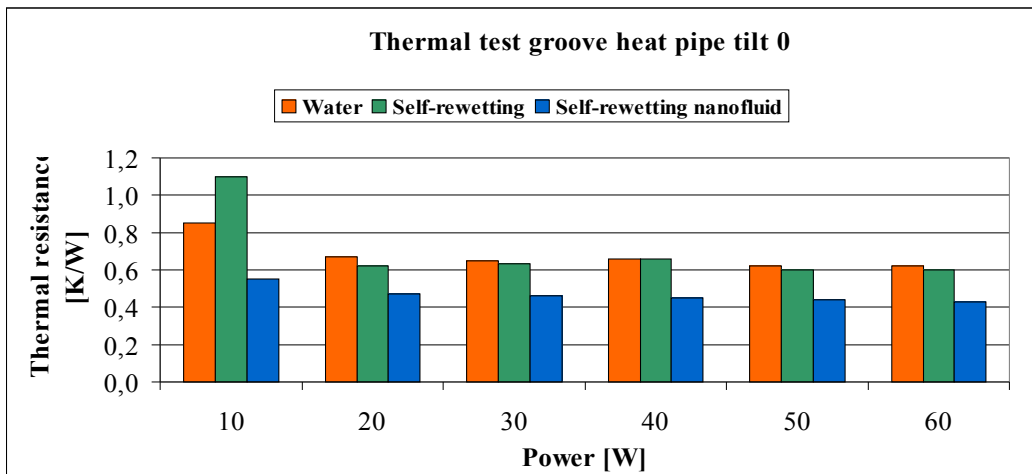


Figure 4-49: Thermal resistance of a groove heat pipe filled with three different solutions

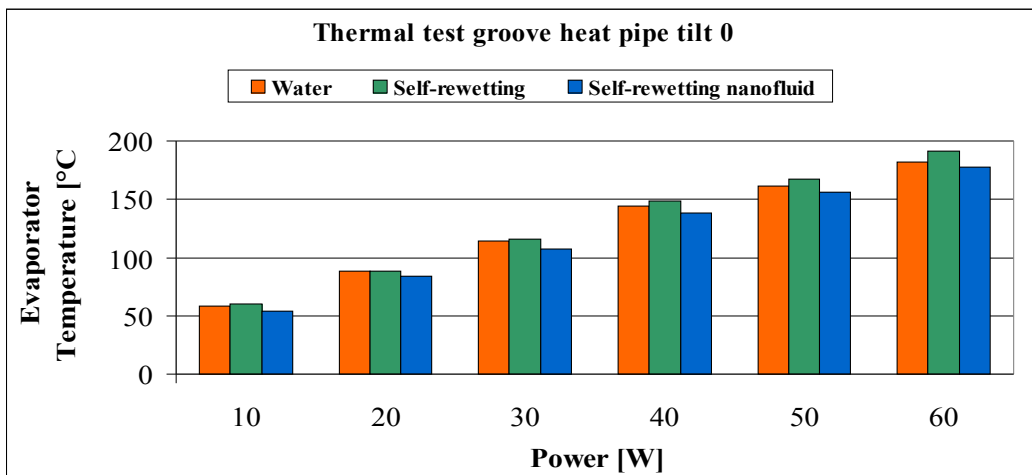


Figure 4-50: Maximum temperature reached to evaporator

Although there are not so much difference between the temperature reached to evaporator, very important results have been found about the use of self-rewetting nanofluids as working fluids, in fact as shown in Figure 4-50 the use of a self-rewetting fluid with this filling ratio does not produce a better thermal resistance and in particular when the power supply is 10Watt the resistance is higher, but using self-rewetting

nanofluids the resistance is better in all range of power supply, this is an important results related to enhanced thermal conductivity.

4.4.3 Effect of filling ratio on thermal test

The main objective of this study is to investigate about the effect of filling ratio in a commercial heat pipe thinking o the evaporator like a dummy cpu, for these reasons the main limi twill be the maximum temperature reached to evaporator (120°C in order to avoid problems realted with a bad-operation of CPU [24]. Figure 4-51 and Figure 4-52 show the results.

Decreasing the filling ratio to 7.5% we have better thermal performances both in term of thermal resistance both in maximum temperature reached, in the case of 5% we have a decreasing of performances with dry-out condition at the power supply of 30Watt: in fact the thermal resistance increase with a power supply of 20Watt and does not reach a steady state condition for 30Watt (T.R.>2 & Maximum Temperature>120°C).

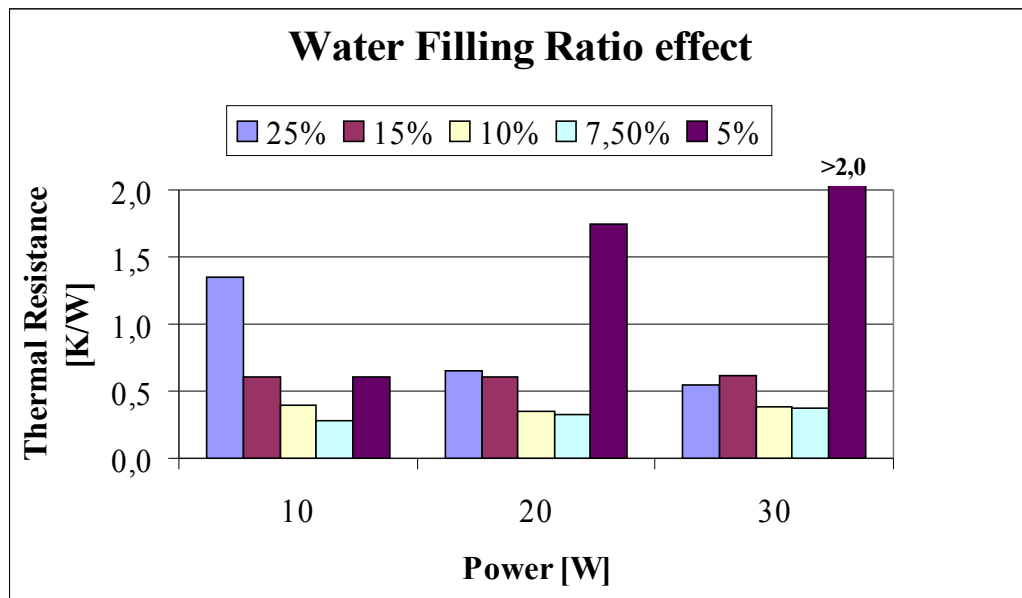


Figure 4-51: Thermal resistance at several filling ratio

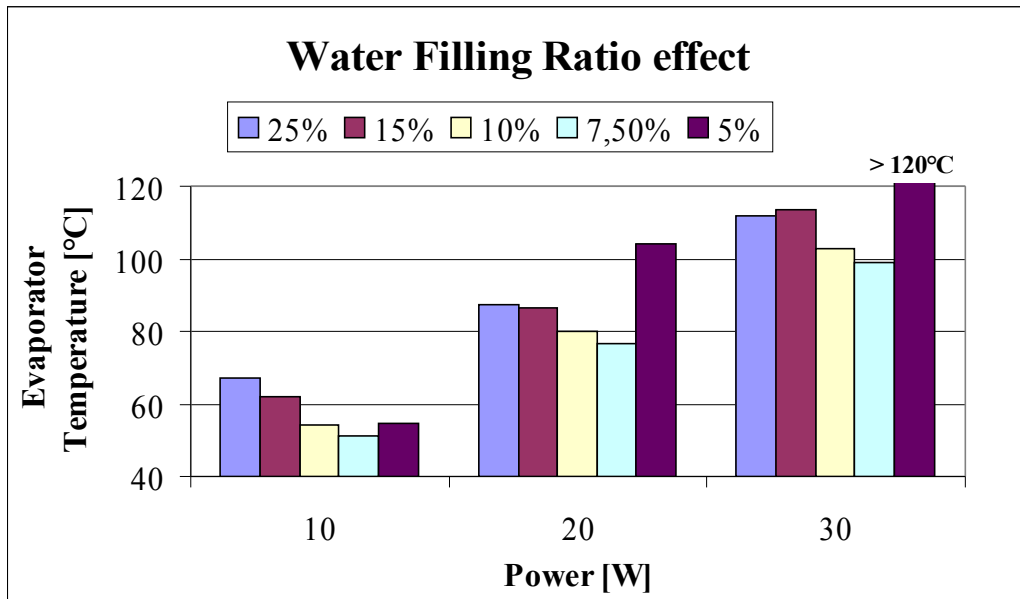


Figure 4-52: Maximum temperature reached at evaporator versus power supply

It is a general opinion that when the filling ratio is enough to saturate the wick structure that is the best filling ratio, in our case the theoretical optimal FR should be 15% but this result is not in agreement with experimental setup.

As already discussed in previous paragraph the mean force in a heat pipe is the capillary pressure drop between the evaporator and condenser, this depends on the meniscus radius generated to the sections and then on the liquid distribution. Due to the evaporation-condensation process the liquid distribution appear as in Figure 4-53 with the more filling zone is obviously the condenser.

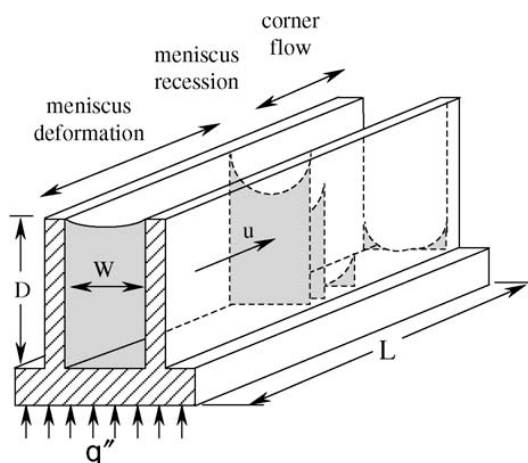


Figure 4-53: Liquid distribution along a groove microchannel [31]

The maximum efficiency has been reached when the liquid meniscus at the condenser is flat and when the capillary force to the evaporator is maximum; the last one affirmation is true when the liquid is in “corner flow” regime (Figure 4-54). This configuration can be reached even if the filling ratio does not guarantee the complete filling of wick structure like experimental result have shown.

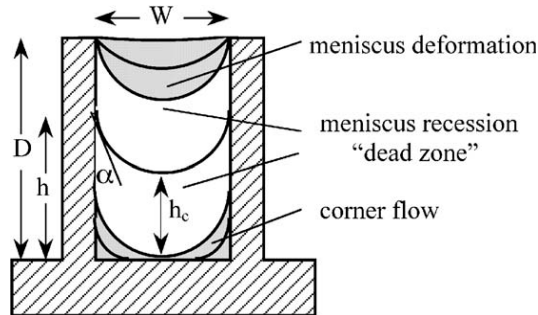


Figure 4-54: Different configuration of liquid meniscus along an axial groove

If we normalize the capillary pressure respect to maximum ($p_c^* = \frac{p_c}{2\sigma\sqrt{W}}$) we can see the effect of a liquid saturation in the channel on this parameter (Figure 4-55).

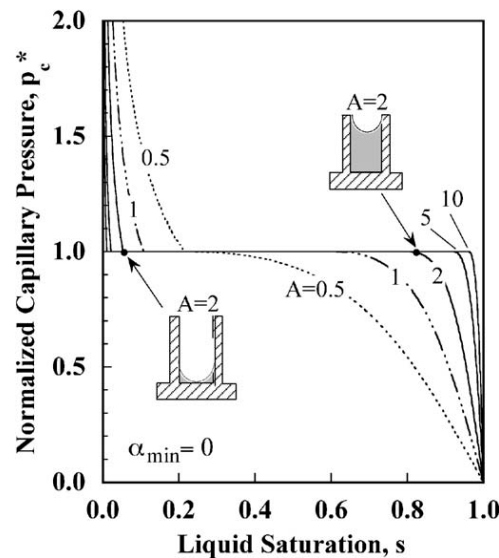


Figure 4-55: Effect of a liquid saturation in a rectangular channel section on normalized capillary pressure at different aspect ratio (A)

An important effect is the dependency of maximum heat flux exchanged versus the aspect ratio and $p_0^* = \frac{p_0}{2\sigma\sqrt{W}}$, when this parameter is equal to zero then we can suppose that the liquid meniscus t condenser is flat, when the value is negative there

will be a ray of curvature of meniscus at condenser section. As aspected the maximum heat flux is higher when $p_0^* = 0$ (Figure 4-56).

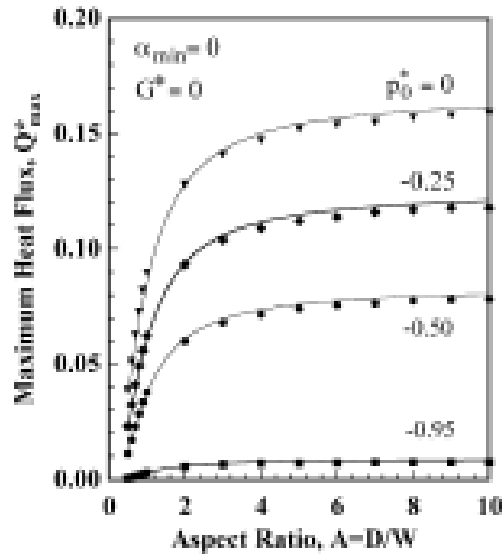


Figure 4-56: Maximum heat flux versus aspect ratio and p_0^*

This dissertation then can explain the experimental results obtained with a filling ratio lower than 15%.

4.4.4 Effect of forced convection on thermal performances

Using the FR of 7.5% a fan has been added to experimental setup, in order to evaluate the effect of forced convection on thermal performances, this setup has been realized with the idea to simulate a correct operation of a modern CPU. In Figure 4-57 and Figure 4-58 are shown the results.

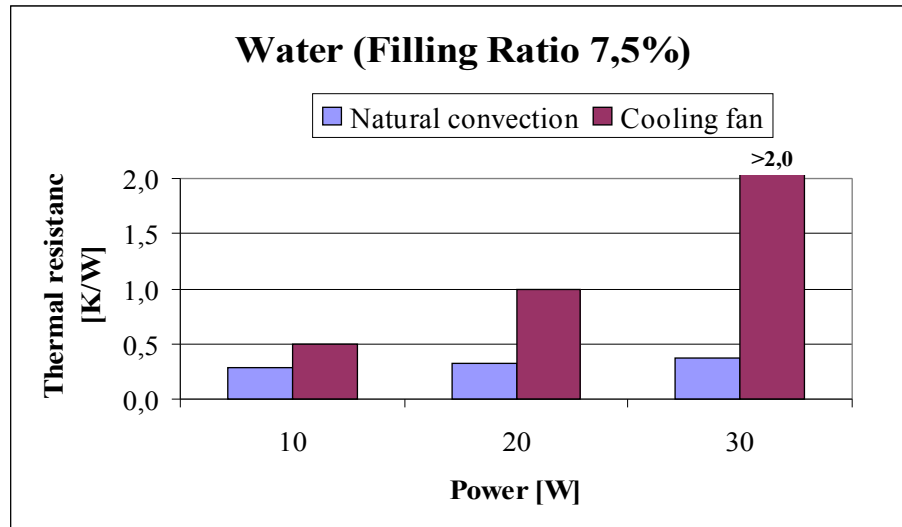


Figure 4-57: Thermal resistance of heat pipe with and without fan

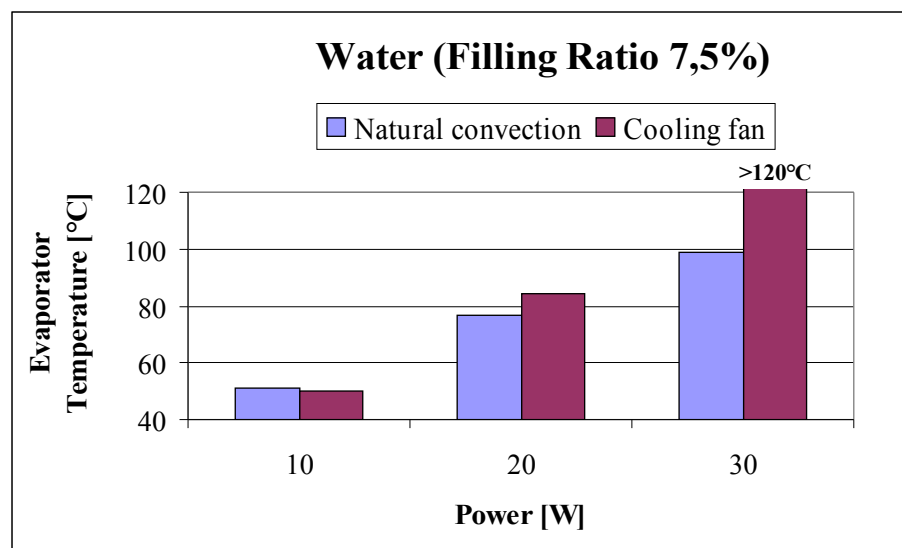


Figure 4-58: Maximum temperature reached in case of natural convection and cooling fan

The temperature reached in the case of forced convection is lower because of the heat exchange at condenser section is higher because the heat transfer coefficient in the case of forced convection is higher. The effect in term of thermal resistance is traduced in fact of this parameter increasing with power supply, because of a strong heat exchange produce also an higher mean velocity of evaporation-condensation with an high pressure drop in the liquid and then an higher thermal resistance.

4.4.5 Comparison between pure water and self-rewetting fluid as working fluid for thermal management of a dummy CPU

It has been experimentally demonstrated as using a self-rewetting fluids instead of pure water in commercial application for thermal management of a dummy cpu is better. Results are shown in Figure 4-59 and Figure 4-60.

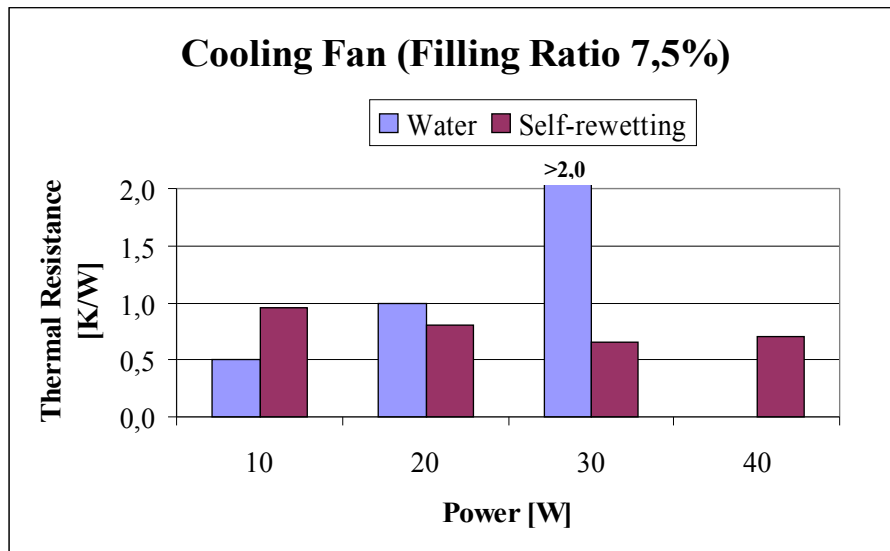


Figure 4-59: Thermal resistance versus power supply for pure water and self-rewetting fluid

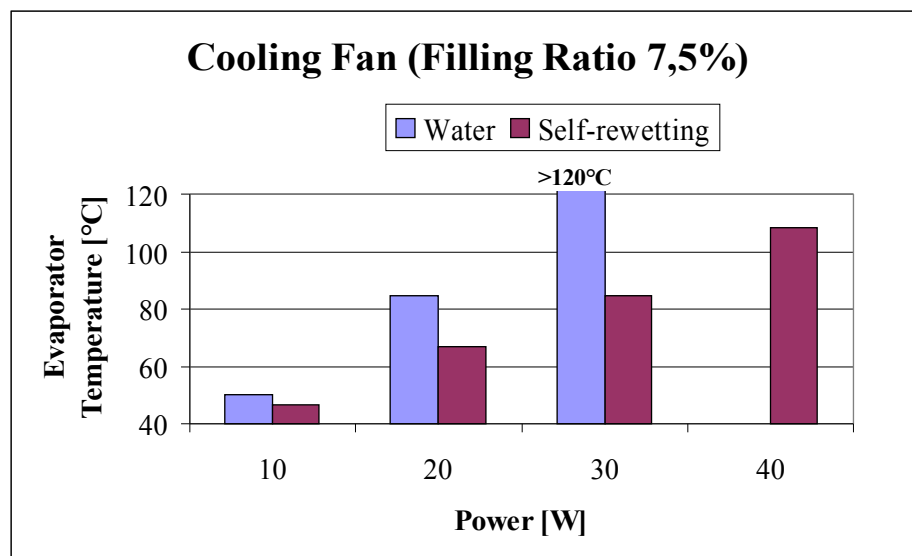


Figure 4-60: Maximum temperature of dummy CPU versus power supply for pure water and self-rewetting fluid

The results show not only a better thermal resistance for the filling with self-rewetting fluid but also the possibility to have an higher power preserving the CPU: in fact the temperature is well lower than 120°C also when the power supply is 40Watt, furthermore the trend of resistance in case of a self-rewetting fluid is decreasing.

Finally we can say that:

- the use of self-rewetting nanofluids improves the thermal performance of heat pipe in term of TR in all range investigated,
- there is an optimum filling ratio in our configuration setup in according with theoretical considerations (7.5%)
- the use of self-rewetting solution for thermal management of a dummy CPU improves thermal performances respect an heat pipe filled with pure water

5 Capillary rising in a laser-engraved capillary structure

5.1 Introduction

Up to now we investigated about different liquid mixtures in the same capillary structure, in particular micro-channels manufactured with the technique of extrusion for a copper tube, in this chapter we will talk about a capillary structure homemade manufactured with a laser engraving technique: 2 different kind of structure have been manufactured and the capillary rising of different mixture have been measured. After the experimental results has also been made a numerical investigation in order to explain these.

5.2 Laser engraving technique

The engraving tests were performed by using a pulsed 30W Yb:YAG fibre laser (Lasit Fly Fiber 30W), with fundamental wavelength $\lambda = 1064$ nm, duration time of 50 ns, pulse frequency variable in the range of 30÷80 kHz, pulse energy up to 1 mJ, was used. The beam is moved through two galvanometer mirrors, and after that the beam is focused by a “flat field” lens with a focal length of 160 mm onto the workpiece. The final focused beam diameter is about 80 μm . The laser system is controlled through a PC, which allows the generation of the geometric patterns and the setting of the process parameters: the average beam power (P_m) by the selection of the maximum pumping diode current percentage (D), the pulse frequency (f) and the scan speed (S).

Before testing the mean power of laser was measured by using a power meter (F150A-SH thermal head and a NOVA display from OPHIR) at different pulse frequency for different diode current. It results in a constant mean power at all frequency corresponding at 10W for D=40%, 16.5 W for D=60, 23W for D=80% and 30W for D=100%. Then, the pulse energy and the pulse power were calculated as the ratio of the average power and the pulse frequency, and the ratio of the pulse energy and the duration respectively, the results are reported in Figure 5-61. In the figure it is possible to observe that both these quantities decrease at the increase of the pulse frequency.

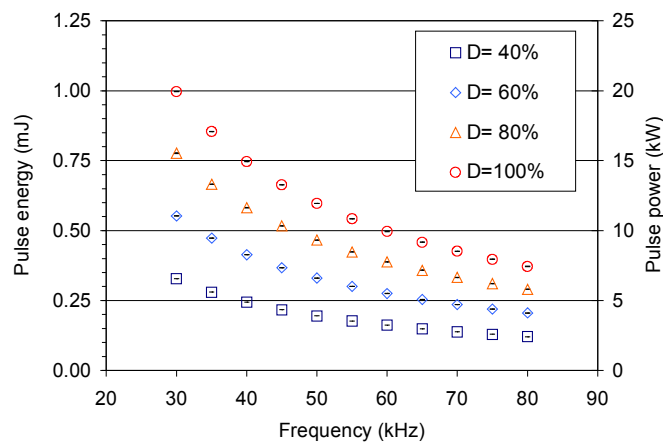


Figure 5-61 Pulse energy and pulse power as a function of the pulse frequency.

Laser surface machining involves several issues which are still poorly understood as they influence material properties and surface morphology as well as the mechanisms by which the surface morphologies are generated. However, the interaction phenomena occurring on the surface are primarily dependent on the total amount of energy released per unit length and on pulse energy as well described in [42-44].

Generally speaking, for a metallic material, the different interaction phenomena change at the released energy per unit length increasing from warm up to melting, then vaporization and steam formation was obtained and finally a reduction of the absorption due to plasma shielding and scatter effect, as reported in Figure 5-62. Furthermore it was shown that at the same released energy per unit length, the use of high pulse energy, assure to achieve highest depth [42,44,-47].

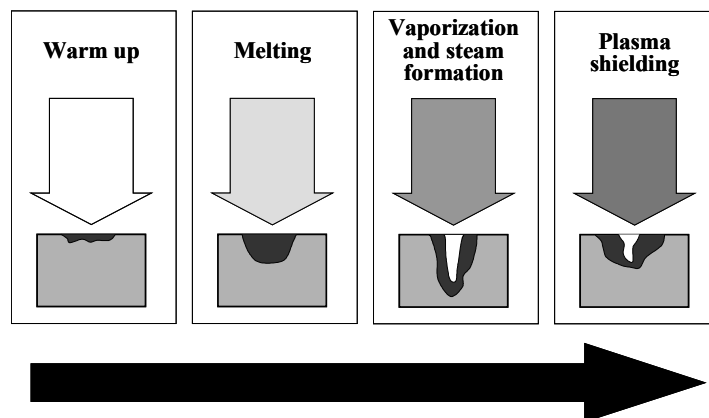


Figure 5-62 Evolution of the interaction mechanism changing the total energy released for unit length.

So in order to achieve high removal rate deepest groove as process parameters it was selected the maximum diode current, that correspond to a mean power of 30W, and the lowest pulse frequency, 30 kHz.

The working speed was selected on the basis of preliminary experiments. In this experiments it was noted that for low beam speed (in the range of 50-400 mm/s) a great amount of melted materials occurs at the edge which solidifies producing spraying, unwanted ejections and bur. Obviously the presence of re-solidified material at the edge of the groove produce an unwanted increase of the roughness inside the groove. So in order to reduce the roughness inside the groove it was used a beam speed of 1200 mm/s. In this condition the reduction of the total amount of the energy per unit length produces a reduction in the bur quantities but also a reduction in the groove depth. Then to obtain a satisfactory depth the operation was repeated more and more times.

To obtain the desired width of the channel two type of strategies were used. In the first case the single channel were obtained repeating 60 times a sequence of 6 parallel linear patterns, 100 mm in length, with a distance between the linear patterns of 25 μm . In the second case the groove were obtained repeating 60 times a sequence of linear pattern, 0.2 mm in length, with a distance between the linear patterns of 25 μm , placed orthogonally the groove axis for a total channel length of 100 mm. In figure 3 it is reported the section of a sequence of 6 channel obtained using the two different strategies. As it is possible to observe, in the first case (Figure 5-63a) well defined triangular shaped channel of 178 μm in depth and 160 μm in width are obtained, while in the second one (Figure 5-63b) reverse trapezoidal shaped channel of 183 μm in depth and 227 μm in width are obtained. As visible in figure 3 in both cases bur is obtained at the channel edge. However in the case of the trapezoidal shape bur occurs also at the channel bottom.

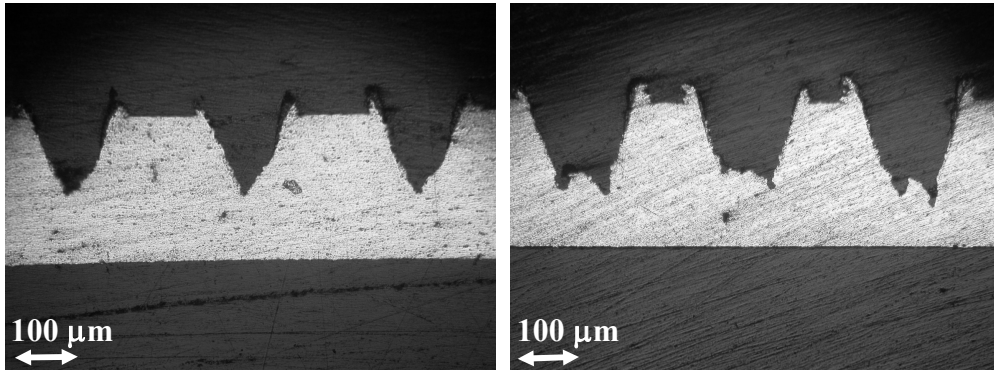


Figure 5-63 Image of the channel section obtained for the two scanning strategies a) first strategy; b) second one.

5.3 *Experimental study on capillary rising in two different groove structures*

In order to check the theoretical model, experiments on capillary rising with ethanol have been carried out. The experimental setup is very simple, the two different grooved structures, that have already been presented in the previous paragraph, have been realized for a length of 150mm, the aluminium foil was immersed in the liquid bath and a ccd camera look in front of the panel (Figure 5-64).



Figure 5-64 A picture captured by CCD camera in the case of capillary rising of ethanol in trapezoidal (on the right) and triangular (on the left) grooves at steady state condition

Ethanol has been chosen because it is a pure liquid almost completely wetting the metal surface (7° contact angle). The capillary height has been evaluated considering the simple equation

$$\Delta P_c = \rho gh$$

Table 5-9 shows the comparison between the theoretical height versus the experimental height for ethanol solution in the either case of triangular and trapezoidal groove.

Capillary rising with pure ethanol		
	Triangular Grooves	Trapezoidal Grooves
Theoretical results	5,0 cm	4,8 cm
Experimental results	5,4 cm	5,3 cm

Table 5-9: Theoretical and experimental results for the capillary rising with pure ethanol

It is clear that theoretical results are in good agreement with experimental results just a little bit higher in the case of experimental heights.

The most interesting results have been obtained in the case of self-rewetting binary mixture and in particular experiments have been performed with a solution of water-butanol at three different concentrations in order to catch the effect of this on the capillary height. (Figure 5-65)

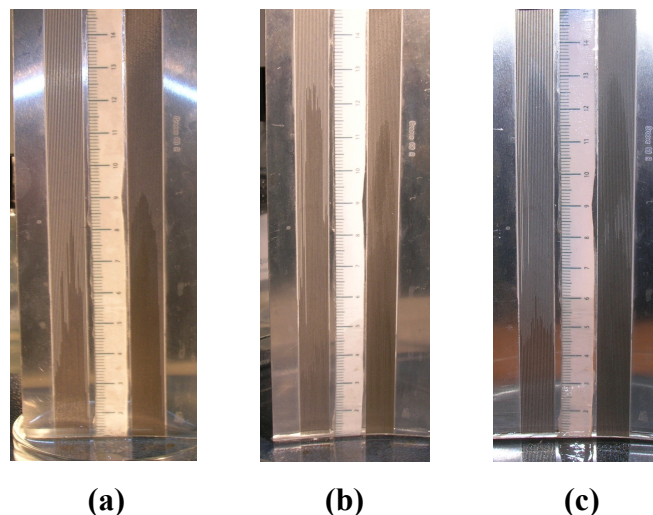


Figure 5-65 Capillary rising at three different concentrations 1wt% (a), 5wt% (b), 7wt% (c) of water-butanol solutions

Looking at Figure 5-65 it is possible to note that for the less concentrated solution the capillary rise is lower for triangular grooves compared to trapezoidal groove and for more concentrated solution the capillary height is, as expected by theoretical predictions, higher for triangular grooves. A possible explanation of this strange behaviour for the solution with less concentration in butanol could be found in literature [48] in fact when the aluminium foil is immersed in the liquid bath it is very important that the liquid go inside the micro-channel and then flows in order to reach the steady state height. In this case we have to take in account another parameter the so called critical angle $\psi=90^\circ-\alpha$, when the contact angle $\theta < \psi$ fluid flow correctly inside the channel, when $\theta > \psi$ fluid do not succeed to do this.

In Table 5-10 the results of contact angle measurements are shown together with the value of ψ in the case of the two different geometries, as waiting in the case of less concentrated solution the condition of no correct flow is respected.

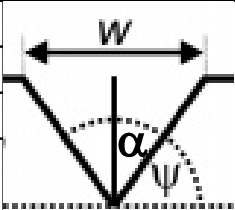
Mixture	θ (°)		ψ (°)	
Water-Butanol 1wt%	80		Triangular	Trapezoidal
Water-Butanol 5wt%	51		77,0	81,5
Water-Butanol 7wt%	42			

Table 5-10 Contact angle measurements for considered mixtures, definition of critical angle and critical angle for triangular and trapezoidal groove

The last consideration is about the relationship between the concentration and the capillary height, in fact it is evident that the capillary height depends on concentrations of solution. Considering that in all cases the experimental capillary rise was higher than theoretical predictions, also 2-2.5 times higher a possible explanation has been given, in particular this strange result could be attributed to three different effects:

- 1) Decreasing of contact angle in micro channels due to surface roughness;
- 2) Increasing of surface tension caused by butanol evaporation;
- 3) Marangoni flow caused by concentrations gradient (“Marangoni tears”).

The first effect is given by the own manufacturer process, in fact the contact angle measurements have been done on aluminium foil before the engraving, it is evident that when the laser engraves surface the roughness changes and is higher. Second effect is almost simple, because it is well known that when the evaporation of the alcohol occurs

the surface tension of the solution is higher because it changes the local concentration of the surfactant alcohol in the water. Third effect it is a strict consequent of the second one, because when the evaporation of butanol occurs the surface tension changes but this phenomena it is not constant in each point of liquid tongue inside the channel: the concentration of the liquid bath reasonable is almost the same compared to the initial condition but it is not true for the top of the tongue where the balance between the butanol that go out during evaporation phase is not balanced by the butanol that diffuse through micro-channel. The gradient of concentration generate a surface tension gradient also, and this is the drive force for a Marangoni flow, that induces an higher pressure at the top of the liquid tongue with the relatively rising of liquid in the channel.

5.4 Numerical results

In order to explain the physical behaviour observed during experiments, very preliminary CFD simulations have been carried out. A 3d computational domain has been investigated with capillary effects in trapezoidal groove. The length is only 5mm because of the computational coast is too high. These simulations are focused only on surface tension gradient effects induced by concentration gradient for Water-Butanol solutions. With an UDF (User Define Function) has been superimposed two different surface tension gradient in the direction of the greater length z (5-10N/m²).

Figure 5-66 shows three different configurations calculated, when the gradient of surface tension is imposed the capillary height is greater as verified in the case of experimental results: in blue is represented the liquid phase with red color is indicated in the air phase.

The authors would highlight as the breakdown of the liquid film in the case of the higher surface tension gradient is not only a numerical results but this phenomenology happened also during the experiments with the solution more concentrated in butanol as right captured by numerical simulation.

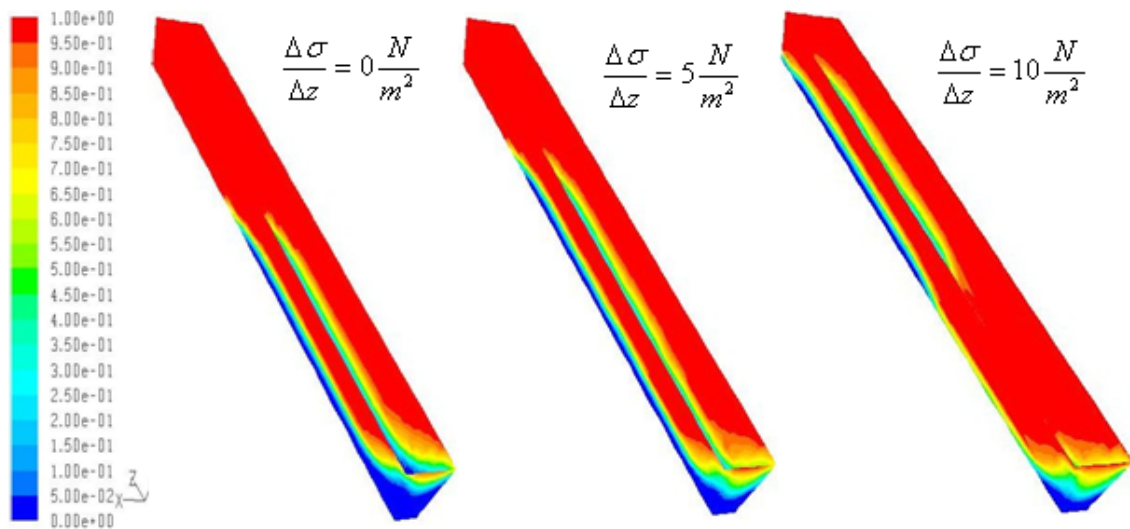


Figure 5-66 Numerical simulations of the trapezoidal microchannel with three different surface tension gradient

In conclusion we can say that in order to study capillary effect in the aluminium laser engraved microchannels experimental tests have been carried out. In the case of binary mixtures of water and butanol, in all cases the measured capillary rising is higher than the expected theoretical results. Possible explanation for this behaviour are:

- Decreasing of contact angle on engraved aluminium surface;
- increasing of surface tension caused by butanol evaporation;
- Marangoni flow caused by concentration gradient on the vapor-liquid interface.

Very preliminary 3D CFD simulations show that increasing the concentration gradient the capillary rise is higher and film breakage occurs.

Complete numerical simulations in the microchannel with real length of 6 cm will be carried out in the future.

6 SELENE Project

6.1 General description

6.1.1 Scientific background and motivation

Increase in size of space platforms and future exploration missions will require a large amount of heat to be dissipated by large space radiators. Efficient thermal control in space, by two-phase closed-loop systems, becomes of crucial importance in these devices. The present research will be focused on the study of the heat transfer performances of binary or multi-component heat transfer fluids with particular surface tension properties and in particular to “self-rewetting fluids”, i.e. liquids with a surface tension increasing with temperature and concentration. Thermophysical properties, like surface tension, wettability and thermal conductivity, at different temperatures, are of crucial importance not only for binary mixtures, but also for a number of ternary aqueous solutions with relatively low freezing point and for nanoparticles suspensions (so called nanofluids). Some of them interestingly exhibit the same anomalous positive surface tension gradient with temperature as binary self-rewetting solutions. Since in the course of liquid/vapour phase change, self-rewetting fluids behaviour induces a rather strong liquid inflow (caused by both temperature and concentration gradients) from the cold region (where liquid condensates) to the hot evaporator region, several interesting applications may be envisaged, e.g. the development of advanced wickless heat pipes for utilization in reduced gravity environments.

The present project intends to contribute to the understanding of the basic fluid dynamic and physico-chemical mechanisms that occur in these multi-component two-phase systems and particularly on the interplay between heat transport and surface and bulk thermophysical properties. To pursue the above objective, the behaviour of non-isothermal self-rewetting liquids will be experimentally investigated under microgravity conditions in transparent heat pipe model systems.

In particular, main objectives include the quantitative investigation of heat transfer performances of self-rewetting fluids in model heat pipes and validation of adequate theoretical and numerical modelling able to predict their behaviour in microgravity

conditions. Once the models have been validated, they can be extended and applied also to terrestrial applications.

In particular, suitable liquid mixtures with surface tension increasing with temperature and concentrations will be compared with reference conventional single-component liquids, in particular water.

Candidate self-wetting fluids include:

a) binary mixtures of water and long chain alcohols (butanol, pentanol, heptanol, octanol, etc at different concentrations (tbd)

b) self-wetting nanofluids, developed as potential future working fluids in heat pipe systems, since their improved thermophysical properties (thermal conductivity, surface tension, contact angle) may increase capillary and thermo-solutocapillary effects and heat transfer performances.

c) low-freezing point aqueous solutions (brines) with self-wetting properties for use in future space heat pipe systems avoiding solidification at relatively low temperature.

6.1.2 Justification for the need of a space experiment

Microgravity offers the opportunity to avoid gravity effects and to analyse in detail typical flow patterns occurring only in the space environment, in relatively large systems, offering the opportunity to perform systematic experimental investigations of the processes, considering a large number of experimental conditions typical of space and terrestrial heat pipes. For this reason the experiments under microgravity conditions can be helpful to focus the attention on

The proposed experiments will use transparent test cells, to allow direct observation, coupled with optical and intrusive techniques to measure thermal/compositional fields. Heat pipes operations are strongly affected by gravity. In general, they are excellent heat transfer devices when operating in gravity-assisted conditions (like thermosyphons), but serious constraints on conventional heat pipes is the reduction of transport capabilities when not gravity assisted. For this purpose, heat pipes utilize the capillary wicking structure to promote the liquid flow from the

condenser to the evaporator and as a result they can also be used in microgravity environments but with very different performances in comparison to normal gravity.

The experiments in microgravity allow one to avoid undesired buoyancy and hydrostatic pressure effects in the liquid and in the vapour phase for almost all experimental conditions and to study only and surface tension-driven effects which are essential for almost all the heat transfer devices based on two-phase flow and capillary effects.

The experiments require very long duration, therefore scientific and technological results can be obtained only on ISS using a dedicated test container.

6.1.3 Detailed objectives

The experiments intend to investigate with onboard available optical diagnostics and other intrusive sensors the main physical mechanisms occurring in different heat pipes systems, e.g. conventional cylindrical or flat heat pipes for terrestrial applications, as well as in thin ultra-light heat pipe radiator panels for potential space applications. Main physical mechanisms that shall be investigated include:

- 1) surface tension-driven and Marangoni flows induced by evaporation, condensation, temperature and concentration gradients
- 2) two-phase flow and liquid and vapour distribution
- 3) Influence of the vapour temperature and pressure
- 4) Influence of the length of the evaporator and/or condenser regions

In particular, simple scaling analysis based on the assumption that the friction pressure losses in the channel are balanced by the capillary pressure only suggests that the maximum dimensionless heat flux at the evaporator/condenser (scaled with

reference thermophysical fluid properties) is proportional to the square of the groove depth to length ratio (L/w):

$$\frac{Q}{(Lw)(\rho H_v \sigma / \mu)} \propto \left(\frac{w}{L}\right)^2$$

where Q is the heat flux density (W/m^2), ρ , H_v , σ and μ are the density, the latent heat of vaporization, the surface tension and the viscosity.

The target of the present research is to model and analyze the evaporation/condensation driven flow in heat transfer devices with maximum heat flux density in the order of $100 \text{ W}/\text{cm}^2$ and w/L in the order $O(10^{-2})$.

The fluid behaviour shall be investigated under different heating conditions (corresponding to different heat power density levels applied at the evaporator section) until dry-out limit is reached. The same experiments shall be carried out sequentially in different cells partially filled with different working liquids, including water as reference single-component and a number of different self-wetting fluids, brines and nanofluids.

Main required measurements include:

- a) heat power provided at the evaporator section
- b) heat exchanged at the condenser section
- c) temperature distributions along the liquid-vapour interface and in the liquid at different positions along the cell (tbd), from the evaporator to the condenser
- d) concentrations in the liquid at different positions along the cell (tbd), from the evaporator to the condenser
- e) liquid distribution and in particular film thickness and shape of the liquid-vapour interface from the evaporator to the condenser using visual observation and quantitative analysis (e.g. interferometric techniques) during heat pipe operations, i.e. from relatively low power up to the dry-out limit for the different investigated working fluids.
- f) flow visualization shall be considered also for liquid velocity measurements.

6.1.4 Experiment concept diagram

SELENE represents a model of heat pipe with capillary structure for investigation of the heat transfer performances (e.g. thermal resistance and maximum heat flux from the evaporator to the condenser) as well as of the basic fluid dynamics and physico-chemical mechanisms occurring in heat pipes when multi-component fluids with anomalous surface tension behaviour are considered.

The facility will contain several heat pipe model systems partially filled on ground after vacuum conditions are established with different fluids. Therefore, according to the available volume, an experiment container with a number of transparent heat pipe model systems shall be developed (Figure 6-67).

The main idea is to enable independent and sequential and/or simultaneous investigations of the different fluid mixtures.

Each cell can be simply a half-heat model with one groove of appropriate cross section shape and size machined into a solid plate. The investigation of the behaviour of the liquid in this groove when the system is subjected to different heat stimuli is the main objective of the experimental research. For each heat pipe, evaporation will be promoted at the hot side (evaporator) with a controllable heater or with a number of heaters located at one bottom side of the groove, while the temperature at the other end (condenser) should be controlled, e.g. by a Peltier elements or by water cooling system. For a given temperature difference, corresponding to a prescribed thermal power, the evaporated liquid will condense at the cold opposite side where heat will be removed by the cooling system and the condensate liquid will be driven back to the evaporator flowing along the channel by the capillary effect and/or by the inverse Marangoni effect.

The different heat pipes will be filled with different liquid alcoholic solutions or multi-component self-wetting fluids. Each pipe will be evacuated and partially filled with liquid before launch.

A set of temperature and concentration sensors shall be mounted on each pipe. In particular micro-sensors for measurements of liquid refractive index should be considered, in order to evaluate the liquid concentration once the temperature is known.

In addition, CCD, Infrared Camera and Interferometric analysis will complete the investigation of the basic fluid physics mechanisms occurring in the heat pipe model. Main objectives will be the quantitative investigation of the liquid-vapour interface shape, of the liquid volume and distribution, as well as of the liquid velocity field.

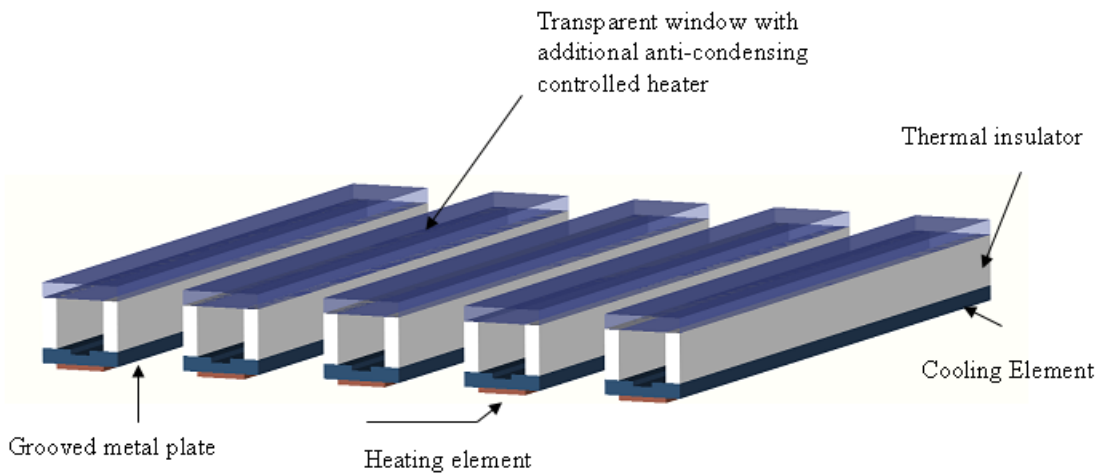


Figure 6-67: Typical layout with 5 heat pipe cells

6.1.5 Shape, structure and size of heat pipe cell

A layout of a possible experimental heat pipe cell is shown in Figure 6-68.

One idea is to have at one side a hydrophilic metallic surface (copper or aluminium) with a dedicated channel (groove) connecting the evaporator to the condenser. The possibility to have a transparent channel to take advantage by possible interferometric systems shall be investigated.

The shape and size of the channel will be designed according to the maximum thermal power and heat flux density, representative of ordinary heat pipes (in the range in the range 0 ~ 200 W, 0-10 W/cm²) but also to allow installation of sensors for local measurements of temperature and/or concentration

The opposite surface of the cell should be made of an optically transparent material with relatively high thermal conductivity (e.g. Saffire) that can be heated and controlled by additional elements at relatively high temperature, to avoid vapour

condensation. The material should be at the same time transparent in the infrared band of a thermocamera that will be selected for measurement of surface temperature. In this way the temperature distribution of the liquid could be evaluated for each experimental condition.

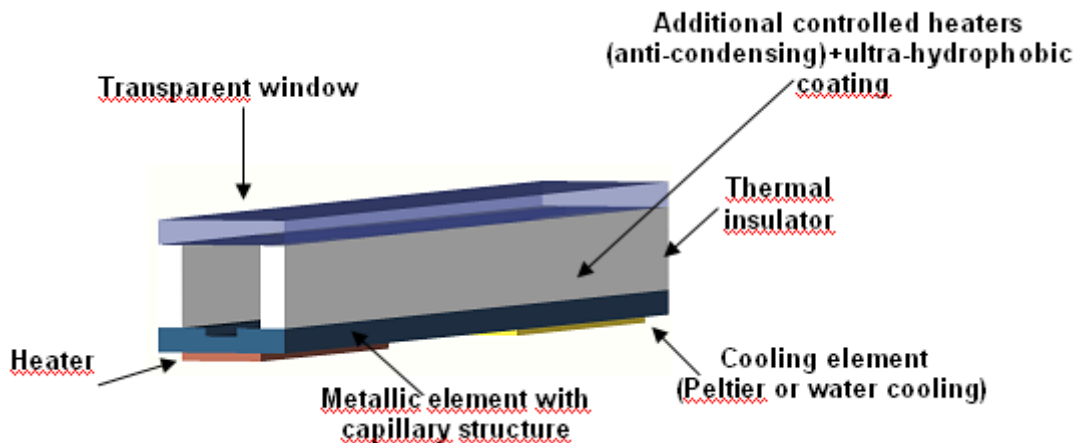


Figure 6-68: Possible heat pipe cell

In microgravity condition, liquid could spread all over the inner surfaces. For this reason, in addition to heating elements to increase the temperature of the transparent surface, a hydrophobic surface will be useful for the cover surface. One possible solution is using a saffire glass coated with hydrophobic coupling agent on vapour side and coated with a transparent electrically conductive thin film heater at the external side. Possible dimensions for the overall heat pipe length, heating region and cooling region are 10-20cm, 20-50mm, 30-60mm, respectively.

The bottom side of the evaporators/condensers may be flat to help mounting heating or Peltier/cooling elements. Possible size of each heat pipe cross section shall be in the range between 5 and 20 mm.

Finally we can say that the experimental apparatus shall be able to perform test with the selected liquid mixtures under different temperature and thermal power conditions (typical temperature range is 0°C-150°C, maximum heat power 200W). For each heat pipe evaporation shall be promoted at the hot side (evaporator) with a controllable heater, while the temperature at the condenser should be controlled by a

Peltier element or by water cooling system. The input heat power at the evaporator shall be controlled for the whole experiment period with a tolerance 0.5 W around the setting value, in the range 0 ~ 200 W. The heating/cooling elements shall be controlled independently and the heat flux at the heating/cooling sections should be measured with an accuracy TBD. The temperature of the cooling section shall be controlled in the range 10°C-80°C.

For a given temperature difference, corresponding to a prescribed thermal power, the evaporated liquid will condense at the cold opposite side where heat is removed by the cooling system and the condensate liquid will be driven back to the evaporator by the capillary structure on the metal sheet and/or by the inverse Marangoni effect.

Additional transparent heating elements shall be used to control the temperature of the transparent cover surface in the range 20°C-150°C. The setting value for the temperature of the cover surface shall be controlled; heat flux provided by these heaters shall be measured with an accuracy TBD.

6.2 Numerical Simulations

As programmed in SELENE project one work-package is related to the numerical simulation about SELENE cell, in particular the main objective of this simulation is to estimate the critical heat flux of the cell: the critical heat flux is the heat flux needed to go to dry-out.

These unsteady numerical simulations have been done with VOF of Fluent, in particular for simulation of evaporation/condensation process has been written an UDF (User Define function): with this function we can introduce a source term in the momentum equation. As first approach the evaporation and condensation has been fixed equal on the interface of the evaporator and condensator and the velocity of evaporation/condensation has been estimated relating to the ratio between heat flux (100Watt) and the latent heat of vaporization of the water. The energy equation has not been added to the set of equation to solve in order to avoid others problem related to the energy balance equation and in particular as first approach.

$$\rho\dot{\alpha} = 10^3 \text{ Kg} / \text{m}^3 \text{ s}$$

The last one is the term that has been added where ρ is the liquid density and $\dot{\alpha}$ is the production of void fraction. In Figure 6-69 has been reported the cross section of the cell with initial condition of liquid distribution.

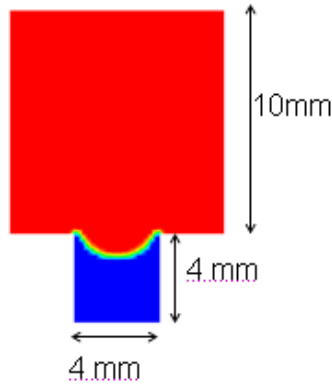


Figure 6-69: Initial liquid distribution in a cross section of SELENE cell

In Figure 6-70 has been reported instead the entire 3D geometry: the length of the cell has been assumed of 15 cm each part (evaporator, adiabatic and condensator region) has been supposed of 5 cm. The use of VOF it has been necessary to take in account of difference of capillary pressure when the evaporation/condensation occurs.

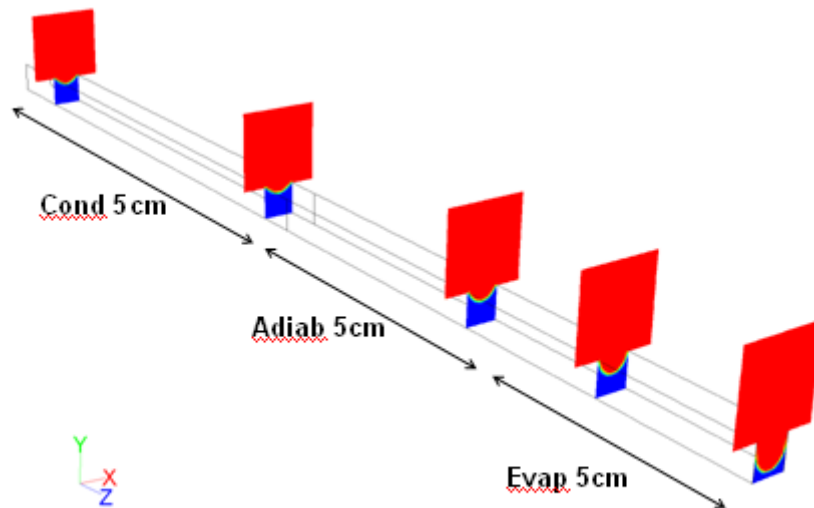


Figure 6-70: 3D geometry and liquid distribution during the simulation



Figure 6-71: Liquid distribution on simmetry plane after 1 and 7 seconds

Region \ Time	Condensator	Adiabatic	Evaporator
1s			
7s			

Table 6-11: Liquid distribution of liquid after 1s-7s in the four different cross section of SELENE cell

In Figure 6-71 and Table 6-11 are summarized the main results of numerical simulation for the SELENE cell with an heat flux of 100Watt; results show that during evaporation/condensation process the amount of liquid in the condensator section increase and correspondingly in the evaporator section decrease, the capillary force due to a minor radius of curvature is more strength but this is not enough for avoiding the dry-out condition that occurs after 7 seconds to initial condition.

It is necessary to take in account that this is the first step in order to simulate the entire process of evaporation/condensation, the first results show that it has been possible to find an heat flux for that the dry-out occurs, the next step will be to simulate the evaporation/condensation process in depend of temperature and pressure parameters in the inner of the cell and then introducing the energy balance equation together with the source term in that equation. In literature there are few works about this problem and it is certain that these results will be the first step for the problem solution.

7 Conclusions

The main objectives of this work have regarded the effects of utilization of self-wetting solution and in particular of nano-self-wetting solution as working fluids in commercial and space heat pipe. These results have been achieved through the experimental measurements of the thermophysical properties and directly test in groove commercial heat pipes in horizontal configuration in order to make a comparison with conventional working fluids. The main activities and results have been:

- Surface tension, contact angle and thermal conductivity measurements has been done for binary and ternary mixture and in particular for self-wetting fluids and nanoself-wetting solutions
- Thermal tests on groove heat pipe has been done and the effect of filling ratio has been studied on the thermal performance, the improvement of using self-wetting and especially nanoself-wetting fluids has been demonstrated in comparison with conventional working fluid.
- An aluminium groove structure has been realized with the laser engraving technique and the solutal Marangoni effect has been studied for self-wetting solution during capillary rising in microchannels.
- The scientific requirements will be defined through theoretical and numerical analyses, as well as experimental ground activities with the objective to identify the flight experimental liquids, the scientific requirements for the flight hardware and the diagnostic systems.

Actually are in progress different activities for using of self-wetting and nano-self-wetting fluids in heat pipe for the modern solar panel and their possible utilization as thermal management of skyscrapers.

In particular has been defined just the base for the Selene Project and in the next future will be carried out, others numerical simulations and experimental setup will be carried out as expected by different WP.

References

- [1] Peterson, G.P., An Introduction to Heat Pipes Modeling, Testing, and Applications, John Wiley and Sons, Inc., 1994.
- [2] Tien, C. L., Fluid mechanics of heat pipes, *Annular Review of Fluid Mechanics* 7,167-185 (1975).
- [3] Cao, Faghri, Simulation of the early startup period of high-temperature heat pipes from the frozen state by a rarefied vapor self-diffusion model, 1993
- [4] Peterson G.P., Analytical development and computer modelling of a bellows-type heat pipe for the cooling of electronic components, *Heat Transfer Engineering*, Vol. 9, No.3, pp.101-109, 1988.
- [5] Hoa C, Demolder B, Alexandre A. Roadmap for developing heat pipes for ALCATEL SPACE's satellites, *Appl Thermal Eng*,2003,23(9):1099-1108.
- [6] Lord Rayleigh, "Capillary action", *Encyclopædia Britannica*, eleventh ed., Cambridge University Press, 1910
- [7] Yoshiyuki Abe, "About of self rewetting fluids- possibility as a new working fluid", *Thermal Science & Engineering* Vol 8 No.4 (2003)
- [8] J.E. Eninger, D.B. Marcus, The Marangoni effect and capacity degradation in axially grooved heat pipes, *Third International Heat Pipe Conference*, Palo Alto,CA,May 22-24, 1978, AIAA Technical paper A78-35576, pp. 14-34.
- [9] M. Kuramae, M. Suzuki, Two components heat pipes utilizing the Marangoni effect, *Chemical Engineering of Japan* 26 (1993) 230-231.
- [10] J.R. Thome, *Enhanced boiling Heat transfer*, Hemisphere Publishing Co., New York, 1990
- [11] Mc Gillis, et al. Western research laboratory Technical Note TN-23, 1992.
- [12] D.M. Pratt, K.P. Hallinan, Thermocapillary effects on the wetting characteristics of a heated curved meniscus, *Journal of Thermophysics and Heat TRAsnfer* 125 (1997) 519-525
- [13] D.M. Pratt, K.D. Kihm, Binary fluid mixture and thermocapillary effects on the wetting characteristics of a heated curved meniscus, *Journal of Heat Transfer* 125 (1997) 867-874

- [14] N. Zhang, D. Chao, Models for enhanced boiling heat transfer by unusual Marangoni effects under microgravity conditions, *International Communications in Heat Mass Transfer* 20 (8) (1999) 1081-1090.
- [15] Rohrer, H., 1996, "The Nanoworld: Chances and Challenges," *Microelectronic Engineering*, Vol. 32, No. 1-4, pp. 5-14.
- [16] Roco, M. C., 1998, "Nanoparticle and Nanotechnology Research in the U. S. A.," *J Aerosol Sci.*, Vol. 29, No. 5/6, pp. 749-751.
- [17] Li, B. C., 1998, "Nanotechnology in China," *J Aerosol Sci.*, Vol. 29, No. 5/6, pp. 751-755.
- [18] Fissan, H. J., and Schoonman, J., 1998, "Vapor-Phase Synthesis and Processing of Nanoparticle Materials (NANO)-A European Science Foundation (ESF) Program," *J Aerosol Sci.*, Vol. 29, No. 5/6, pp. 755-757.
- [19] Hayashi, C., and Oda, M., 1998, "Research and Applications of Nano-Particles in Japan," *J Aerosol Sci.*, Vol. 29, No. 5/6, pp. 757-760.
- [20] S.U.S.Choi, ASME-FED 231, 99 (1995)
- [21] X. Q. Wang, A. S. Mujumdar, *International Journal of Thermal Sciences* 46, 1 (2007)
- [22] B.C. Pak, Y.I. Cho, *Experimental Heat Transfer* 11, 151 (1999)
- [23] Y.M. Xuan, W. Roetzel, *Int. J. Heat Mass Trans.* 43, 3701 (2000)
- [24] Y. Xuan, Q. Li, ASME *J. Heat Trans.* 125, 151 (2003)
- [25] S. K. Das, N. Putta and W. Roetzel, *Int. J. Heat Mass Trans.* 46, 851 (2003)
- [26] S. J. Kim, I. C. Bang, J. Buongiorno, L. W. Hu, *Appl. Phys. Lett.* 89, 153107 (2007)
- [27] C. Y. Tsai, H. T. Chien, P. P. Ding, B. Chan, T. Y. Luh, P. H. Chen, *Materials Letters* 58, 461 (2004)
- [28] S-W kang, W-C Wei, S-H Tsai and S-Y Yang, *Applied Thermal Engineering* 26, 2377 (2006)
- [29] Y-H. Lin, S-W. Kang, H-L. Chen, *Appl. Therm. Eng.* 28, 1312 (2008)
- [30] V. Contini, R. Mancini, R. Marazzi, D. Mirabile Gattia, M. Vittori Antisari, *Phil. Mag.* 87, 1123 (2007)
- [31] D. Mirabile Gattia, M. Vittori Antisari R. Marazzi, *Nanotechnology* 18, 255604 (2007)

- [32] M. Vittori Antisari, D. Mirabile Gattia, R. Marazzi, E. Piscopiello, A. Montone, in *Nanotubes, Nanowires, Nanobelts and Nanocoils-Promise, Expectations and Status*, edited by P. Bandaru, S. Grego, I. Kinloch (Mater. Res. Soc. Symp. Proc. Volume 1142, Warrendale, PA, 2009), 1142-JJ05-16.R1
- [33] R. Prasher, D. Song, J. Wang, *Appl. Phys. Lett.* 89 (2006) 133108-1-3.
- [34] RS Data sheet Thermocouples
- [35] Adamson, A.W. *Physical Chemistry of Surfaces*, 2nd Edition, Wiley, interscience, New York, 1967
- [36] Bashforth, S.; Addams, J.C. *An attempt to test the Theory of Capillary Action*, Cambridge University Press and Deighton, Bell and Co, London, 1882
- [37] Andreas, J.M.; Hauser, E.A.; Tucker, W.B. *J. Physical Chemistry*, 1938
- [38] Girault, H.H.; Schiffrin, D.J.; Smith, B.D.V. *J. Colloid interfaces Sci.*, v.93 p.169, 1984
- [39] Huh, H.; Reed, R.L. *J. Colloid Interface Sci*, 1983
- [40] R. G. Miller and L. S. Fletcher, *proceedings of the Tenth Southeastern Seminar on Thermal Sciences*, New Orleans, LA, 1974 *_unpublished_*, pp. 263–285
- [41] H. Ziebland, in *Thermal Conductivity*, edited by R. P. Tye *_Academic*, London, 1969_, Vol. 2, pp. 96–110.
- [42] A. Kaldos, H. J. Pieper, E. Wolf, M. Krause. *Laser machining in die making - a modern rapid tooling process.* *J. Mat. Proc. Tech.*, 155-156:1815-1820, 2004
- [43] J. Qi, K.L. Wang, Y.M. Zhu, “A study on the laser marking process of stainless steel” *J. of Materials Processing Technology* Vol. 139 2003, pp. 273–276.
- [44] C. Leone, S. Genna, G. Caprino, I. De Iorio, (2010), “AISI 304 stainless steel marking by a Q-switched diode pumped Nd:YAG laser”, *J. of Materials Processing Technology*, *Journal of Materials Processing Technology*, (2010), Vol. 210/10, pp. 1297–1303
- [45] C. Leone, R. E. Morace, I. De Iorio. *AISI 304 Stainless Steel Engraving by Q-Switched Nd:YAG Nanosecond Laser.* *J. Chin. Soc. Mech. Eng.*, 28(2):217-224, 2007.
- [46] N.M. Bulgakova, A.V. Bulgakov, *Pulsed laser ablation of solids: transition from normal vaporization to phase explosion*, *Applied Physics A: Materials Science & Processing*, V. 73, 2001, pp. 199–208.

- [47] S. Genna, C. Leone, V. Lopresto, L. Santo, F. Trovalusci, “Study of fibre laser machining of C45 steel: influence of process parameters on material removal rate and roughness”, *International Journal of Material Forming*, Volume 3, Supplement 1/April, 2010, pp. 1115-1118.